Preparation and Evaluation of Pyropheophorbide *a* Derivatives

Beibei Feng

MSc by Research

University of York

Chemistry

December 2016

Abstract

Photodynamic therapy (PDT) is an approved treatment for a wide range of diseases, especially for cancer. The essential elements in the treatment involve light source with appropriate wavelength, photosensitizing agents and oxygen in tissue. With minimally invasive ability, it attracts increasing attention and most of which centered in the development of efficient photosensitizers (PSs).

Several pyropheophorbide *a* derivatives, such as 2-(1-hexyloxyethyl)-2-devinyl pyropheophorbide (HPPH), with preferred properties have already progressed into clinical trial as potential photosensitizer (PS) candidates, inspired by which, this study used pyropheophytin *a* as starting material in the preparation of five derivatives of pyropheophorbide *a,* with four of them believed to be novel compounds, pyropheophorbide *a* 1-octadecanol ester (**3a**), pyropheophorbide *a* 2-methoxyphenol ester (**3c**), triglycine ester of **3a** and **3c** (**6a** and **6c**).

Compounds synthesized in this work has been confirmed by ^{1}H-NMR and MS. The UV-vis spectra, MS^n, RP-HPLC and solubility measurement were also applied to compare the behavior of the five compounds. The three pyropheophorbide esters have identical maximum absorption wavelength (665 nm in red range). The pair of C-3[1] modified components also have identical absorption maxima (660 nm in red range). Although the three pyropheophorbide esters possess similar structures, their MS^n dissociation behaviour shows several differences. For example, the loss of entire 2-methoxyl phenol group was observed in MS^2 of the methoxyphenol ester, leaving a carbonyl residue on C-17[3] where an acid group remained in MS^2 of the octadecanyl and cholesteryl esters.

RP-HPLC and TLC behavior gave consistent polarity trends for the five derivatives: (1) the triglycine derivatives exhibit greater polarity than the phaeophorbide esters; (2) **3c** and **6c** are more polar than **3a** and **6a**, respectively; (3) pyropheophorbide *a* cholesterol ester (**3b**) demonstrated identical polarity behavior with **3a**. The more polar compounds **6a** and **6c** exhibited greater solubility in the polar solvent methanol than **3a-c**, and when increasing the solvent polarity (introducing 50% water), only **6c** showed weak solubility.

List of Contents

List of Tables

List of Figures

Acknowledgements

Great appreciation and thanks must be given to my dear supervisor Professor Brendan Keely. Thanks to his guide, help and encouragement with lots of patience during the research, the work presented in this thesis was able to be completed as expected. I would like to give my sincere thanks to my TAP member Dr. Anne Routledge for her invaluable suggestions to my research and report writing.

Moreover, my special thanks also go to Heather, Karl and Ed for their training support and help during practical analysis of NMR and MS.

During the Master year, many suggestions and assistance from my colleagues Cezary and Marina are appreciated. In addition, I also want to thank other members of the BJK group for their support during this memorable and meaningful year: Scott, Adam, Yige, Alex and Martina. It was lucky and pleasure to work with you all.

The in-time assistance and nice attitude from departmental staff Rachel, Steve, Jing and Leonie is appreciated.

In the end, my infinite love and thanks would be given to my darling Rui, my parents, brothers and my best-in-the-world families. Thank you very much for your love and support all the time!

Author’s Declaration

I declare that this thesis is a presentation of original work and I was the sole author. This work has not previously been presented for an award at this, or any other University. All sources are acknowledged as References.

1. Introduction

1.1 Photodynamic therapy

Photodynamic therapy (PDT) is a clinically approved treatment for a range of diseases from skin conditions such as chromoblastomycosis (1) to cancers: non-small cell lung cancer, for instance.

Three essential elements are involved in PDT: light of an appropriate wavelength, a light-sensitive agent, photosensitizer (PS) and oxygen in the tissues. The PS can be either applied topically *i.e.* in the treatment of actinic keratosis (AK), a skin condition, or injected intravenously to circulate systemically (2). After a certain period in a light-free environment, the administered PS is allowed to accumulate in the malignant organs whereas it is eliminated from or metabolized by healthy cells. This is followed by the illumination of the diseased skin either directly or focused on the cancerous region *in vivo, via* an optic fiber, for instance. The topical or focused light application aims to avoid undesired destruction to other normal tissue, which is also the reason that the patients have to remain in the dark for days after the treatment, allowing the residual PS to be removed from the healthy tissues.

On absorbing energy from the specific light source, the PS is promoted from the ground state (S0) first to its activated singlet state (S1). This short-lived S1 state either releases energy through generating fluorescence or thermal dissipation or it forms the triplet state (T1) *via* inter-system crossing. The T1 state, which has a high activity, reacts in one of three ways: 1) gradual decaying by phosphorescence; 2) Reaction Ⅰ： ① transfer of hydrogen atoms or electrons to biomolecules, such as nucleic acids, lipids and proteins, ② forming reactive oxygen species (ROS) including superoxide anion $O_2^{\cdot -}$, hydroxyl radical $OH^{\cdot}$ or hydrogen peroxide H_2O_2, *via* interaction between O_2 and the PS radical; 3） Reaction Ⅱ： directly transferring its energy to $^3O_2$ (natural triplet state of O_2), giving rise to the highly reactive singlet state $^1O_2$ (3). Two additional pathways have been suggested to contribute in PDT treatment as well, causing damage to blood vessels of tumor tissues, thereby preventing the cancer from receiving necessary nutrients, and activation of the immune system to attack tumor cells (4).

1.2 Outline of PDT

1.2.1 Development of PDT

The application of PDT dates back to as far as 3000 years ago when the Egyptians, Indians and Chinese employed light to irradiate psoralen (5), a photoactive component in the seeds of *Psoralea corylifolia* to treat the skin disease known as vitiligo (6). The concept of "photodynamic" was first proposed by Professor Hermann von Tappeiner in 1904 when he made his first attempt to use a variety of dyes， such as eosin (a xanthene dye) as the PS in the treatment of skin diseases (7), obtaining positive results.

In 1908, hematoporphyrin (Figure 1.1), an endogenous substance, was found to be sensitive under the illumination of violet-blue light and photo-toxic in mice, leading to damage to red blood cells and paramecia (8). Five years later, Doctor Meyer-Betz tested photodynamic therapy on himself through exposure to sun after injection of 200 mg hematophorphyrin (9). He experienced the symptoms of swollen face, muscle pain, weakness and brown urine for two months. In 1942, localization studies conducted by Auler and Banzer showed that there were different retention times for hematoporphyrin between normally functioning and cancerous cells (10), confirming its potentially practical utility in clinical treatment. Since then, research into hematoporpyrin and its derivatives in PDT treatment has been prevalent. In recent years, PDT study has gained unprecedented popularity due to its unrivalled advantages: less damage to normal issues and minimal invasive ability.

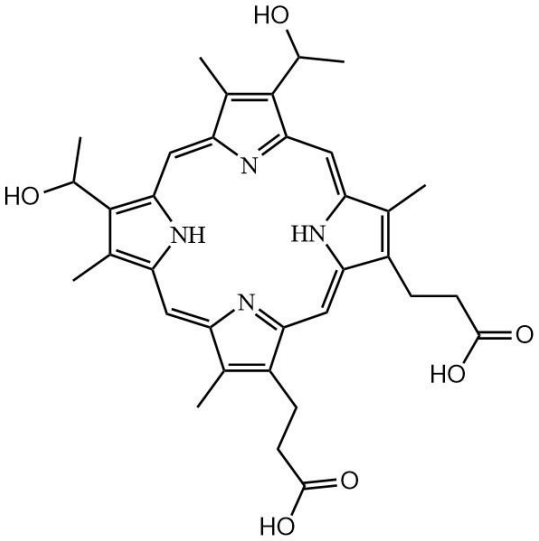

Figure 1.1 Hematoporphyrin

1.2.2 The development of photosensitiser

1.2.2.1 First generation

(1) Hematoporphyrin derivatives (HpD)

Hematoporphyrin (Hp) and its Zn complex was used in treatment of cancer in the 1940s. Due to its poor localizing ability, improved hematoporphyrin derivative (HpD), a mixture of monomers, dimers, and oligomers, was synthesized through the treatment of Hp with AcOH/H_2SO_4 (11). The active component in the HpD mixture was believed to be the dihematoporphyrin ether (DHE, Figure 1.2) (12). The development of HpD underpins todays research about PDT, so it is known as the first generation of PS (13).

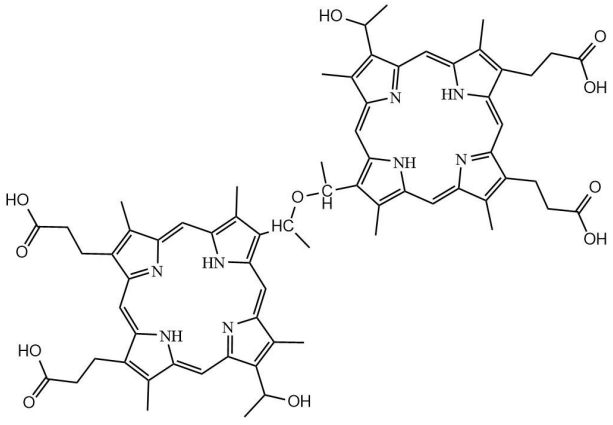

Figure 1.2 Dihematoporphyrin ether (DHE)

(2) Porfimer sodium

Porfimer sodium (Photofrin®, Figure 1.3), the first approved PDT drug in Canada in 1993, was used in the treatment of bladder cancer. This was followed by it being marketed in Japan (1994, for early stage lung cancer), and in the U.S (1995, esophageal cancer; 1998, non-small cell lung cancer; 2003, Barrett's esophagus) (14). Freitag et al. (15) reported that after the application of porfimer sodium and brachytherapy treatment all 32 patients with non-small cell bronchogenic carcinoma and bulky endobronchial tumours recovered, and 28 patients did not show any further symptom of residual or local recurrent endobronchial cancer. That porfimer sodium is classified as a first generation PS is probably because of its complex existence as HpD.

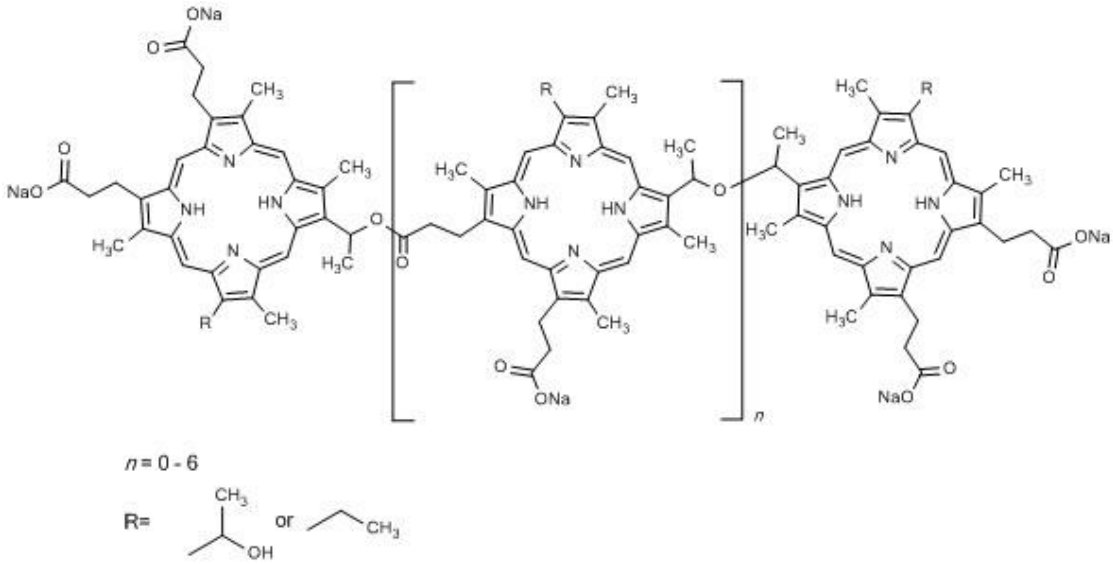

Figure 1.3 Porfimer sodium

Porfimer sodium has low absorption efficiency (ε_{max} ~3,000 $M^{-1}cm^{-1}$) at its maximum wavelength 630 nm, and shallow penetration depth (2-3 mm), which limits its application to surface malignant regions. After treatment with porfimer sodium, patients have to remain in the dark for six to ten weeks due to its long-term skin phototoxicity. On the other hand, the high quantum yield (Φ = 0.89) of singlet oxygen ($^1O_2$) produced by Photofrin secured general permission worldwide for its use in clinical applications.

Photogem® and Photosan-3®

Two other hematoporphyrin derivatives, Photogem® and Photosan-3®, have been registered for clinical use in Russia and the EU, respectively. Bae, *et al.* reported that Photogem® cause tumor cell necrosis and plasma membrane damage as the main mechanism in PDT treatment to cancerous tissue (16).

1.2.2 Second generation

A new generation of PS with low skin toxicity, strong absorption at higher maximum wavelength and greater penetration ability has become the priority target in the development of PDT.

(1) Porphyrin derivatives

Aminolevulinic acid (ALA, Figure 1.4, a) and its methyl ester (MAL, Figure 1.4, b) represent another type of PDT medicine from the porphyrin family (Figure 1.4). They are, in most cases, involved in topical treatment and have been used to treat a number of skin diseases (17). Both substances are absorbed through the skin, are metabolized and then act as precursors in the biosynthesis of protoporphyrin IX (PPIX, Figure 1.4, d), a photosensitive substance belonging to the porphyrin family. MAL (Metvixia®) is approved in several countries and is applied in the clinical treatment of nonhyperkeratotic actinic keratoses of the face and scalp. It has the additional strength of better lipophilicity and deeper skin penetration than ALA. Moreover, reports indicate that ALA and MLA both play significant roles in the treatment of other dermatological conditions such as inflammatory diseases (Acne vulgaris, Hongcharu *et al.* (18); Pinto *et al.* (19)), as well as microbial diseases (for example Leishmaniasis (20,21)) due to their excellent cosmetic outcomes.

The maximum absorption wavelength for PPIX ranges from violet (400 nm) to red (630 nm). The light sources for ALA, MAL involved treatments are approved to be at 400 nm (ε_{max} ~ 40,000 $M^{-1}cm^{-1}$) and 630 nm (ε_{max} ~ 5,000 $M^{-1}cm^{-1}$), respectively. The former offers highest efficiency (Φ = 0.56) while the latter provides deeper tissue penetration (22). Another type of ALA ester, hexaminolevulinate (HAL, Figure 1.5, c) has been used in the diagnosis of bladder cancer since its approval by the USA FDA in 2010, and more applications are ongoing. Research (23) showed that it is 50

to 100 times higher than ALA in converting to PPIX.

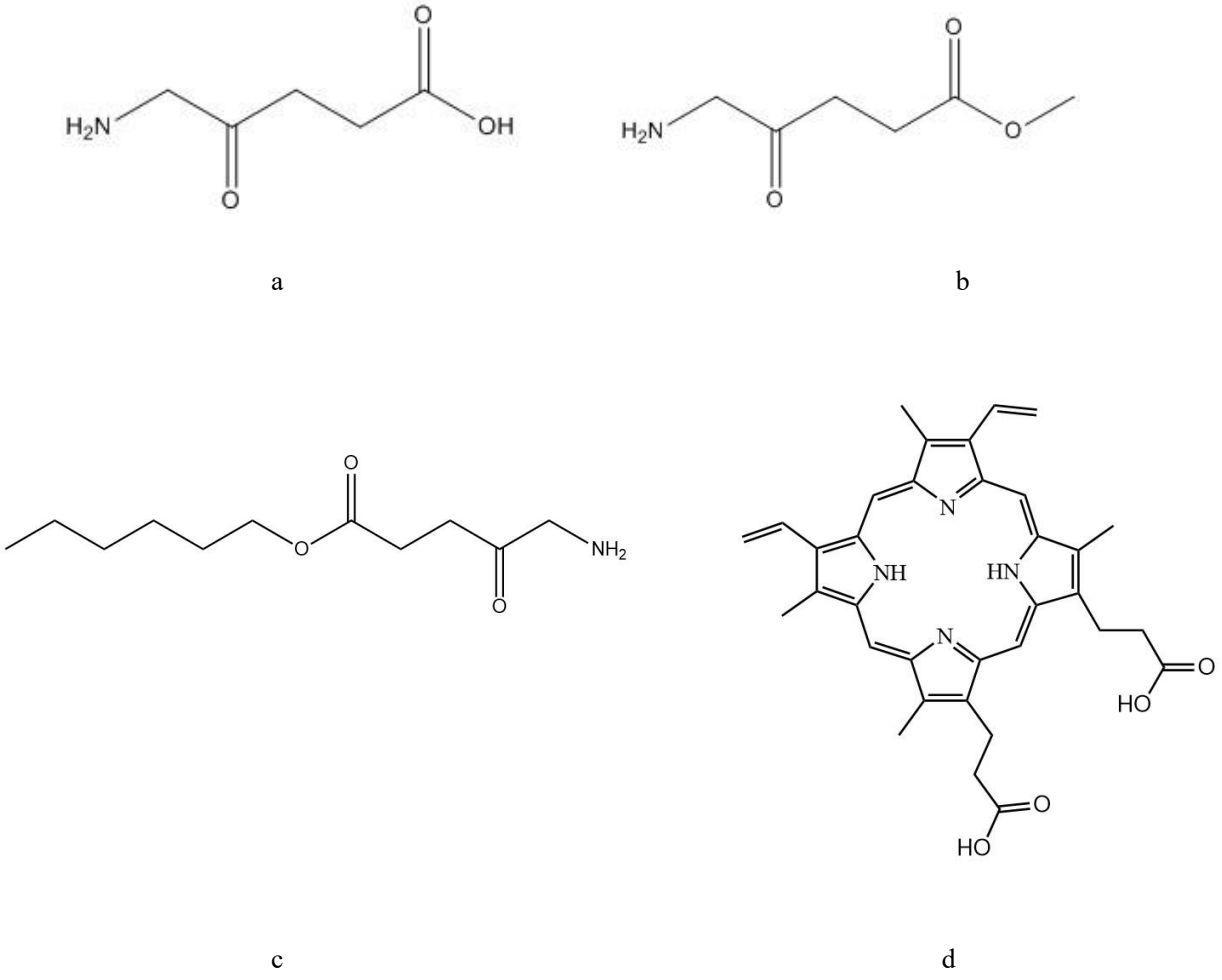

Figure 1.4 Chemical structures of ALA (a), MAL (b), HAL (c) and PPIX (d).

(2) Chlorin derivatives

Chlorins are members of the porphyrin family in which a double bond in one of porphyrin rings has been saturated (Figure 1.5). Consequently, chlorins show a red shift in the absorption spectrum (640 to 700 nm) in comparison with porphyrins. Several compounds derived from chlorins have been developed and applied, or are under clinical trial, in treatments for a wide range of diseases, especially for oncology research.

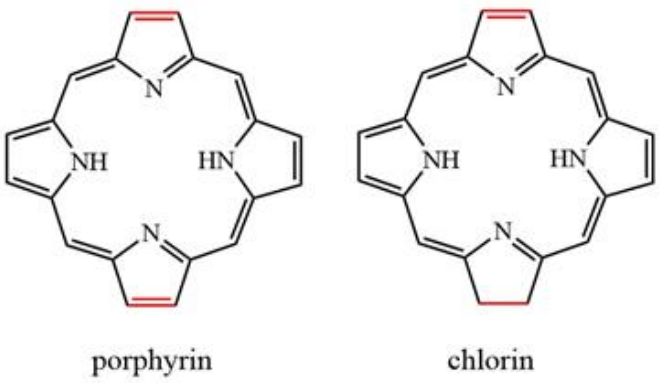

.Figure 1.5 Comparison on basic structural difference of two dyes.

These derivatives include benzoporphyrin derivative monoacid ring A (BPD-MA, Figure 1.6), meta-tetra-(hydroxyphenyl) chlorin (*m*-THPC, Figure 1.6), tin ethyl etiopurpurin (SnET2, Figure 1.6), and *N*-aspartyl chlorin e6 (NPe6, Figure 1.6). The absorption wavelength, pros and cons, and medical applications of these PSs are listed in Table 1.1.

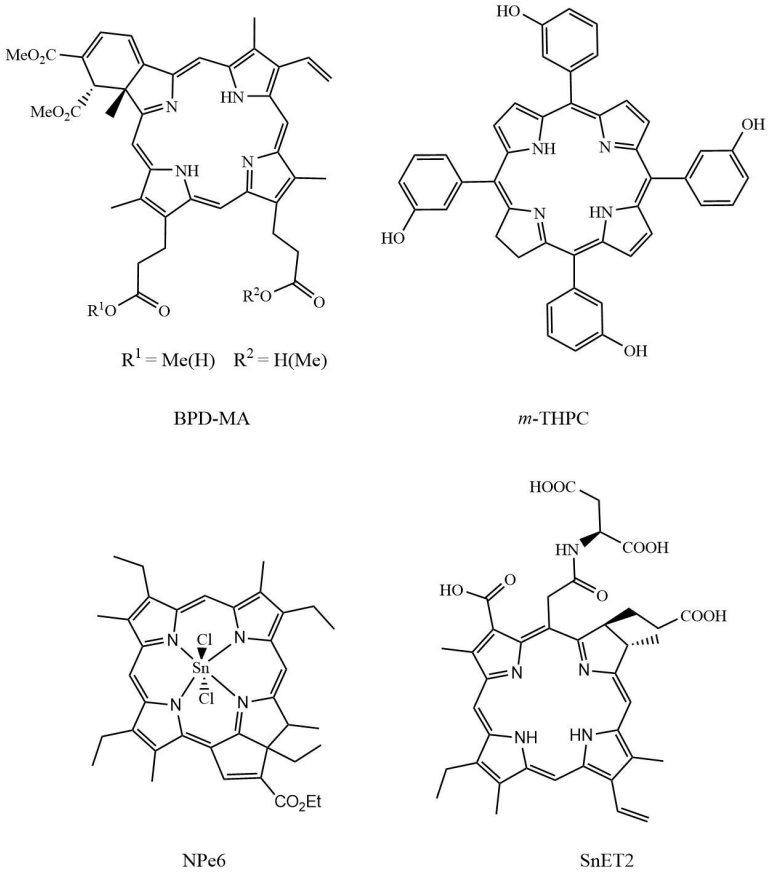

Figure 1.6 Chlorin derivatives

Table 1.1 Properties of some photosensitizers derived from chlorins.

Name	Absorption wavelength	Advantage	Disadvantage	Application
BPD-MA	689 nm	Lower skin phototoxicity, high efficiency (Φ = 0.84) (24)	–	Age-related macular degeneration (FDA, 1999 Visudyne®) (25)
m-THPC	652 nm	High efficiency (Φ = 0.87)	high skin phototoxicity	Breast, prostate, pancreatic cancers (25-27). Neck and head cancer (Europe, Foscan®)
SnET2	664 nm	Deeper tissue penetration	Skin phototoxicity, dark toxicity	Metastatic breast adenocarcinoma, basal cell carcinoma, and Kaposi's sarcoma (Phase I/II) (28)
NPe6	664 nm	Lower skin phototoxicity	–	Lung cancer (Japan, 2003) (29,30)

(2) Pyropheophorbide derivatives

Pyropheophorbide, retaining the chlorin structure, possesses an extra ring in addition to the four pyrrole rings. It can be prepared by acidifying chlorophyll. In common with many other chlorin derivatives, it has a prominent absorption maximum in the red range as well as the main Soret band. For instance, 2-(1-hexyloxyethyl)-2-devinyl pyropheophorbide (HPPH, Photochlor®, Figure 1.7) absorbs at 665 nm with ε_{max} ~47,000 $M^{-1}cm^{-1}$ (31). HPPH has not been approved for treatment yet, but many clinical trials and Phase I/II trials for esophageal cancer (32), basal cell skin cancer (33), lung cancer (NCT0528775) and esophageal cancer at precancerous or early stage conditions have been proceeding.

Lobel. *et al.*(31) injected HPPH (0.5 mg/kg) into nude rats with brain tumors to study its pharmacokinetics and PDT effects. They found that the tumor-to-brain drug ratios ranged from 5:1 to 15:1 after 24 h. They also reported that the attenuation

depth of light at 665 nm used to activate HPPH is approximately 30% greater than that of light at 630 nm used to activate Photofrin in athymic rats normal brain tissue. These results identified the potential use of HPPH as an adjuvant for the treatment of malignant gliomas.

It is worth mentioning that the work in this thesis involved the preparation of several pyropheophorbide derivatives and consideration of their properties. The details are discussed in later chapters.

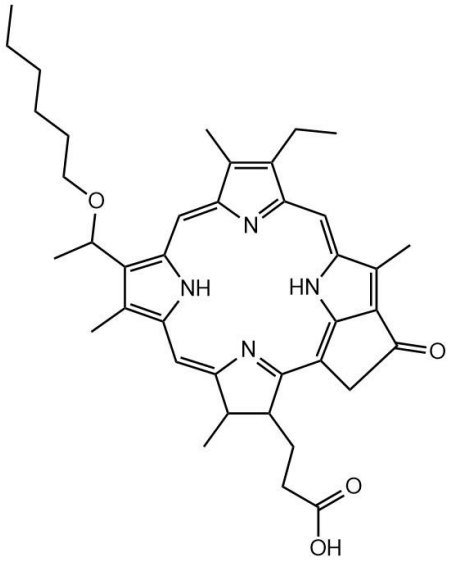

Figure 1.7 2-(1-hexyloxyethyl)-2-devinyl pyropheophorbide (HPPH)

1.2.3 Third generation

Increasing the targeting ability of photosensitzers is attracting researchers' attention in modern PDT research. The advantages of this strategy lie in the high utilization ratio of drugs, hence reducing their administered dose and minimizing the potential damage to healthy tissues. Moreover, in the physiological environment, drug-incorporated delivery systems were proved to be able to reduce self-assembly and aggregation of some photosensitizers, such as those from the pheophorbide family (34). Several reports have considered the factors that affect the delivery efficiency of conjugating drug-carrier systems. Kerdous *et al.* (34) studied the mechnisms of transfer of the conjugate between pheophorbide-*a* (Pheo) and poly (ethyleneglycol-b-Ɛ-caprolactone) to MCF-7 cancer cells and membrane models. They reported increasing delivery efficiency and found the majority of the drug was transferred directly *via* the cell membrane, followed by the release from nanoparticle carriers on contact of the carrier with the cancer cells ("collision"). They further suggested that a minor delivery process might involve the internalization of a small amount of the nanoplatforms by the cells. Therefore, they concluded that there were multiple mechanisms by which systemic delivery drugs exited simultaneously and that the balance between these was likely to depend on the properties of the drug/ polymer couple as a whole. Although the research regarding drug targeting ability in PDT has shown some positive results and is receiving increasing attention, its practical application in cancer treatment is still limited as the relevant research is quite recent.

1.3 Properties of ideal PDT drugs

1.3.1 Strong absorption in appropriate wavelength range

It is preferable to apply red light (650-850 nm) as the illuminating source in PDT treatment. It reduces the disturbance of endogenous pigments and the light scattering that occurs with irradiation using lower wavelengths, both of which lower the efficiency of absorption by the active PS (35). Higher wavelengths have lower energies, hence the energy may not be sufficient to generate active oxygen species with the desired toxic effects (36). In addition, when the wavelength of irradiation increases to higher than 900 nm, the photo flux reaching the tissues is reduced and the internal temperature within the tissue is increased because of enhanced absorption by

water molecules (37).

The extinction coefficient (ε_{max}) of ideal PDT drugs should be high, e.g., 50,000–100,000 M^{-1} cm^{-1} (32) under the irradiation conditions employed. HPPH, which has its maximum absorption at 665 nm (ε_{max} ~ 47,000 M^{-1} cm^{-1}, in vivo) (31) has been approved for use in clinical trials for esophageal cancer (38).

1.3.2 High quantum yield of toxic oxygen species

Desirable photosensitizers must have the capacity to produce adequate levels of ROS, one of the key criteria for potential PDT efficacy (35). The singlet oxygen quantum yield (Φ_{Δ}) is defined as the number of singlet oxygen molecules generated for each photon absorbed by the PS (39). Ormond *et al.* (32) reported that the singlet oxygen quantum yield (Φ_{Δ}) of Photofrin® is 0.89 (λ_{max} = 630 nm), known to be the highest value among the porphyrinoid family.

1.3.3 No dark toxicity and no impact to normal organs and tissues

In addition to possessing strong light absorption capabilities, potential PDT drugs should have no or minimal toxicity in the absence of light. For instance, it has been claimed that porfimer sodium exhibits no systemic toxicity, carcinogenicity or mutagenic activity at the doses used (40). Due to their high dark toxicity, metal-containing complexes cannot be viewed as good PDT candidates (41).

1.3.4 Selectivity of damage and targeting ability

It is generally demonstrated and acknowledged that PDT drugs themselves have the capacity to accumulate ultimately in irregularly growing cells (42), which contributes to a shift away from conventional tumor treatment (43). Moreover, selectively targeting against the tumor tissues without affecting normal organs would be a preferred strategy for PDT treatment, as a result of which the administered dose accumulation period before the therapy and possible toxicities caused by residual PS, for example to skin and eyes, could be greatly reduced.

Protein conjugating system

Since 1975 when Nobel Prize holders Kohler and Milstein invented the hybridoma technology (44), the production of monoclonal antibodies (MAbs) has been realized. Following the lead of this invention, modern PDT development can use antibodies that conjugate effectively with the PS. In general, the process of MAbs production can be described as follows. After injecting a specific antigen to the mouse, B cells provoked by the immune system produce corresponding antibodies that have bonding ability to the antigen. The desired antibodies that are harvested are used to conjugate with PSs, so that this combination is ready to target malignant cells possessing corresponding antigen ligands.

The direct conjugation between PS and antibodies was mediated by interactions between functional groups on amino acid side chains of the antibodies, including thiols (SH) or amines (NH_2), and designed activating groups on drug percursor molecules *via* carbodiimide coupling agents or reductive amidation as appropriate. The first PS-antibody targeting couple was produced *via* the carbodiimide coupling agent by Levy's group in Canada. They reported the binding percentage reached up to 60% (45), much higher than was expected, because of the high volume of the active group (NH_2) on the antibodies.

However, researchers were not satisfied with this achievement, so increasing types of carrier have been developed. One of them is the commonly used drug vehicle, liposomes. The antibody generated through the hybridoma technology targets an antigen attached to the T-lymphocytes. Yemul *et al.* (46) bonded this antibody to the photosensitizer pyrene, contained in liposomes, and found the bonding ratio between pyrenyl groups and antibodies reached 400: 1. In treatments with these antibody-lipsome-PS conjugates, B-cell and T-cell lines were generated *via* irradiated immune system. Although the former was cleared soon after, the surviving T-cell lines confirmed the validity of this approach.

Another member in the protein family with targeting ability is low density lipoprotein (LDL) that helps carry cholesterol, the in demand and key component of biological membranes, especially in malignant tissues due to their hyperproliferation (47). Therefore, the diseased cells developed a higher volume of LDL receptors than

normal cells. Because of its large playload lipid structure, LDL is believed to be able to extensively incorporate within most hydrophobic PSs (48).

Non-protein ligand conjugating system

The antibody induced targeting system has a major downside - high cost, which inspires the development of alternative cost-effective ligands with targeting ability.

A multifunctional drug delivery system based on gold nanoparticles (AuNPs) has been introduced and researched by Dixit, *et al.* (49) These dual-targeted AuNPs [(epidemical growth factor peptide + transferrin peptide)-AuNPs] bound with the overexpressed epidemical growth factor and transferrin receptors, respectively, in glioblastoma cells, increasing the efficiency of delivering the hydrophobic photosensitizer phthalocyanine 4 (Pc 4) to a brain tumor by a factor of 5-6 fold. In addition, the specificity for tumour cells was enhanced and the time of maximal accumulation was reduced compared with single-targeted AuNPs (epidemical growth factor peptide-AuNPs) (49). Another robust multifunctional nanocarrier, (Fe_3O_4-NS-C_3N_4@mSiO_2-PEG-RGD), was confirmed (50) to have abilities to target cancer cells through both peptide- and magnetism-mediated targeting, increasing the amount of drug reaching the cancer cells and releasing the anticancer drugs in the lower pH environment (4.5-5.5 in cancer cells). When loaded with photosensitizer and applied together with chemotherapy, it showed improved inhibition of the growth of A549 and HeLa cancer cells.

Liposomes systems are a traditional drug delivery vehicle that has been modified to become a qualified PDT agent carrier, effectively increasing the proportion of drugs in malignant tissues against that in normal tissue.

1.3.5 Chemical purity and stability

Photosensitizers should be of high chemical purity, so the mechanisms of action can be easily understood and the potential adverse effects recognised. Furthermore, they should be chemically and physically stable for safe and easy shipping and storage (51).

1.4 Review of the localization research for photozensitizers

The ratio of PS taken up by carcinoma cells or healthy tissues determines the treatment efficiency for PDT. As the ROS have short life-times they take effect close to the site of their generation, hence the subcellular localization preference of the PS plays a crucial role in the drug delivery strategy and illumination approach for clinical practice. In this section, the understanding and development of PS localization principles at the subcellular level is reviewed.

As structure determines property, so likewise the structure of the PS governs the nature of its transferrance in the physiological environment and its distribution pathway in cells. To be specific, three structural features that induce interactions with differing locating sites are widely acknowledged: 1) the degree of hydrophilicity; 2) the charge status; 3) the degree of asymmetry. Subcellular distribution sites that accumulate most PS involve lysosomes, mitchondria, plasma membrane, Golgi apparatus and the endoplasmic reticulum (52).

Hydrophilicity

Hydrophobic chemicals are normally carried by LDL when passing through the plasma membrane, known as endocytosis, while hydrophilic substances undergo pinocytosis, a type of endocytosis, by which cells gather external substances into special membrane-bound vesicles contained within the cell, followed by transporting and releasing them on the other side of cell membrane.

Rück *et al.* (53) used the chorioallantoic membrane of fertilised eggs as surrogates for cancer cells to show that lipophilic drugs accumulated in high concentrations in endothelial cells of vessels whereas hydrophilic drugs cleared from the vessels but accumulated in cancer cells instead.

As mentioned in Section 1.2.2, *m*-THPC is a promising second generation PDT drug. Its use was, however, rejected by the FDA with one of the reasons being its non-specific location in cells due to its high symmetrical structure (four identical *m*-hydroxyphenyl groups on the methene bridges: meso- positions). To understand the relation between structure property and the distribution preference, Wiehe *et al.*

(53) prepared 21 meso-substituted porphyrine derivatives (Table 1.2), and compared their solubility, fluorescence lifetimes (τ_F) and oxygen quantum yields (Φ_Δ) in ethanol with that in dipalmitoyl phosphatidylcholine (DPPC) liposomes. As expected, compounds containing *m*-hydroxyphenyl substituents (compounds 14-21, Table 1.2) reached the highest concentrations in ethanol, which was only observed for compounds 16, 19-21 (Table 1.2) with three or four *m*-hydroxyphenyl substituents on the meso- positions. On the other hand, as indicators of the localization of the dyes in the lipid bilayer (54), the fluorescence lifetime and oxygen quantum yields of 19-21 showed a decreasing trend (τ_F =6-7 ns, Φ_Δ = 0.16-0.18) comparing with others (τ_F =9-13 ns, Φ_Δ = 0.23-0.33). These results could possibly be attributed to the structural distinction: three hydrophilic groups (hydroxylphenyl) and one hydrophobic chain (pentyl, hexyl and heptyl, respectively) on 19-21, localizing preferably in the hydrophilic/hydrophobic interface of liposomes given their amphiphilic property. This study demonstrated that the localization priority can be realized through the specific structural modification introduced.

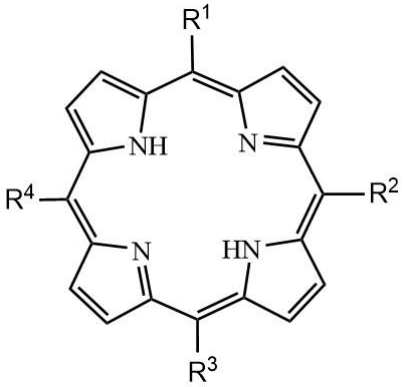

Table 1.2 Meso-substituted porphyrine derivatives

No.	R^1	R^2	R^3
1	H	*iso*-butyl	hexyl
2	H	*iso*-butyl	H
3	H	hexyl	H
4	Hexyl	H	3-methoxyphenyl
5	H	3-methoxyphenyl	hexyl
6	pentyl	3-methoxyphenyl	3-methoxyphenyl
7	hexyl	3-methoxyphenyl	3-methoxyphenyl
8	heptyl	3-methoxyphenyl	3-methoxyphenyl
9	H	3-methoxyphenyl	4-aminophenyl
10	hexyl	3-methoxyphenyl	4-aminophenyl
11	H	3-methoxyphenyl	H
12	H	3-methoxyphenyl	3-methoxyphenyl
13	3-methoxyphenyl	3-methoxyphenyl	3-methoxyphenyl
14	H	3-hydroxyphenyl	H
15	H	3-hydroxyphenyl	3-hydroxyphenyl
16	3-hydroxyphenyl	3-hydroxyphenyl	3-hydroxyphenyl
17	hexyl	H	3-hydroxyphenyl
18	H	3-hydroxyphenyl	hexyl
19	pentyl	3-hydroxyphenyl	3-hydroxyphenyl
20	hexyl	3-hydroxyphenyl	3-hydroxyphenyl
21	heptyl	3-hydroxyphenyl	3-hydroxyphenyl

Charge status

Related research reported that compounds with two, or more than two, negative charges tend to be taken up by lysosomes, which was proved by Woodburn's location tendency study (55) in V79 Chinese hamster lung fibroblasts and C6 glioma cells. The candidate portfolio included hematoporphyrin (HP) and photophyrin IX derivatives with structurally modified substituents, showing hydrophobic and anionic or cationic properties at physiological pH. The authors found that anionic

compounds tended to accumulate in lysosomes, while their counterparts with net positive charge more often distributed in mitochondria.

Asymmetry

As mentioned before, part of the reason that *m*-THPC was denied licence for use in clinical trials was its non-specific intracellular distribution, which is substantially accounted for by its highly symmetrical structure.

Kessel *et al.* (56) studied the localisation of two meso-tetraphenylporphyrin derivatives: a) 5, 10-di[4-*N*-trimethylaminophenyl]-15, 20-diphenylporphyrin (DADP-a, Figure 1.8); b) 5, 15-di[4-(*N*-trimethylaminophenyl)-10, 20-diphenylporphyrin (DADP-o, Figure 1.8). Both structures carry two cation groups (N-$(CH_3)_3^+$) on the *p*-phenyl positions. They found the former dye accumulated mostly in mitochondria, while the latter one accumulated mostly in lysosomes, which was attributed to their difference in degree of asymmetry, with the DADP-o as the more symmetric molecule.

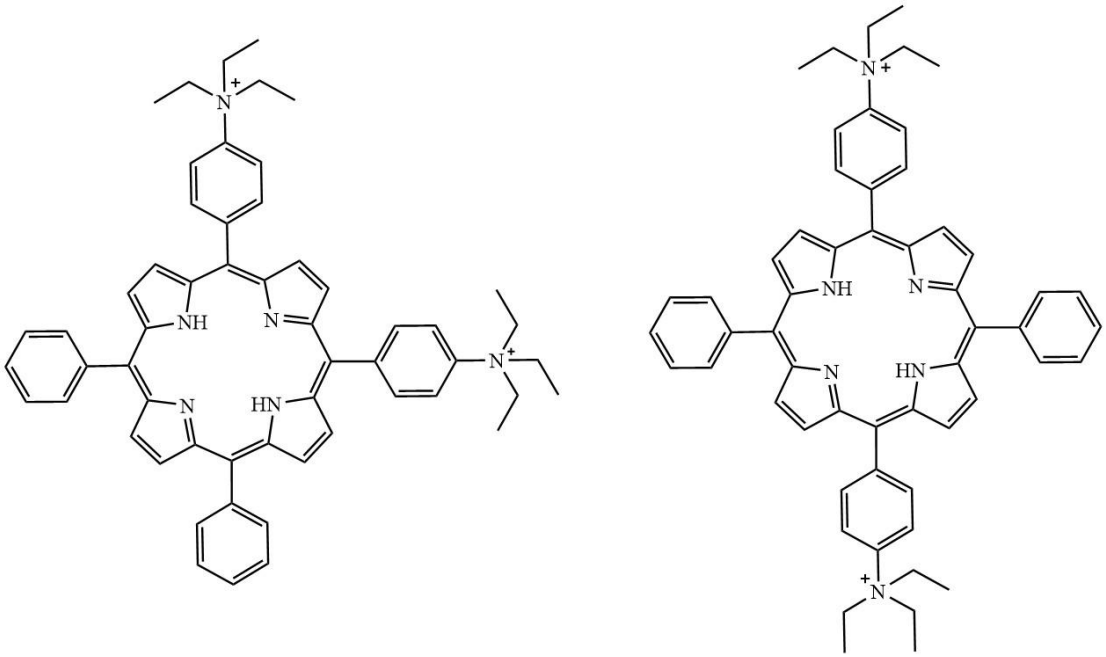

Figure 1.8 5, 10-di[4-N-trimethylaminophenyl]-15, 20-diphenylporphyrin (DADP-a) and 5, 15-di[4-(N-trimethylaminophenyl)]-10, 20-diphenylporphyrin (DADP-o)

Table 1.3 lists the differences among three subcellular locating sites in terms of the photosensitizing efficiency and localisation priority, as well as a few drug preparations for each site.

Table 1.3 Comparison on several locating sits in cells.

Locating sites	Photosensitizing Efficiency	Locating Priority	Locating Instances
Lysosomes	Low (due to aggregation Tendency)	A critical intracellular target for localization (57)	−2 or greater charge. Chlorin based PS: chlorin (e6), ATX-S10 (Na) (58)
Mitochondria	High	A critical intracellular target for localization (59)	Cation charge. polycationic liposomal BPD (60,61)
Plasma membrane	-	Uncommon locating site, main locating site for some dyes	Deuteroporphyrin IX (DP) and its monobromo and dibromo derivatives (62)
Golgi apparatus and endoplasmic reticulum	-	Uncommon locating site, main locating site for some dyes	Foscan®

The distributions for photozensitizers vary with changing conditions, such as the incubation time. For instance, the phthalocyanine (Pc 4) localized in the majority of cytoplasmic membranes, including mitochondria, lysosomes and Golgi apparatus, in the first hour after administration to LY-R cells (63). In the following two hours, the concentration of Pc 4 in lysosomes was reduced and the amount increased in the Golgi apparatus and the mitochondria.

Although the understanding of location tendency for photosensitizers has been developing, it is still fragmentary and further research about its influence in PDT treatment is still required.

1.5 Research objectives

The overall aim of this study was to prepare and characterise a range of pyropheophorbide *a* derivatives incorporating various esters at the C-17^3 position as well as with the modification on C-3^1 positions potential candidates for PDT and to compare the impacts of the modificaitons on the solubility of the chlorins. Evaluation of their effectiveness as photosensitisers was beyond the scope of the study. Specific objectives were:

(1) prepare and characterise a variety of C-17^3 esters (Chapter 2);

(2) prepare and characterise derivatives of pyropheophorbide *a* esters modified at C-3^1 by incorporation of triglycine (Chapter 3);

(3) examine and compare the solubility of these chlorin derivatives in solvent mixtures of different polarities (Chapter 4).

2. Pyropheophorbide *a* esters

As stated in section 1.2.2 (2), pyropheophorbide *a*, carrying one extra ring compared to chlorin, was tested to have maximum absorption wavelength (665 nm, Table 2.3) in the desired range (650-850 nm, Section 1.3.1). In this chapter, three ester chains from distinctive families, including aliphatic hydrocarbon (**3a**), sterol (**3b**) and aromatic hydrocarbon (**3c**), were incorporated to the propionic acid residue of pyropheophobide *a*. With the different chains on C-17^3 position, the behavioral differences in respect of the ultraviolet-visible (UV-vis) absorption, multistage mass spectrometry (MS^n) and polarity as well as solubility can be examined and compared as a whole.

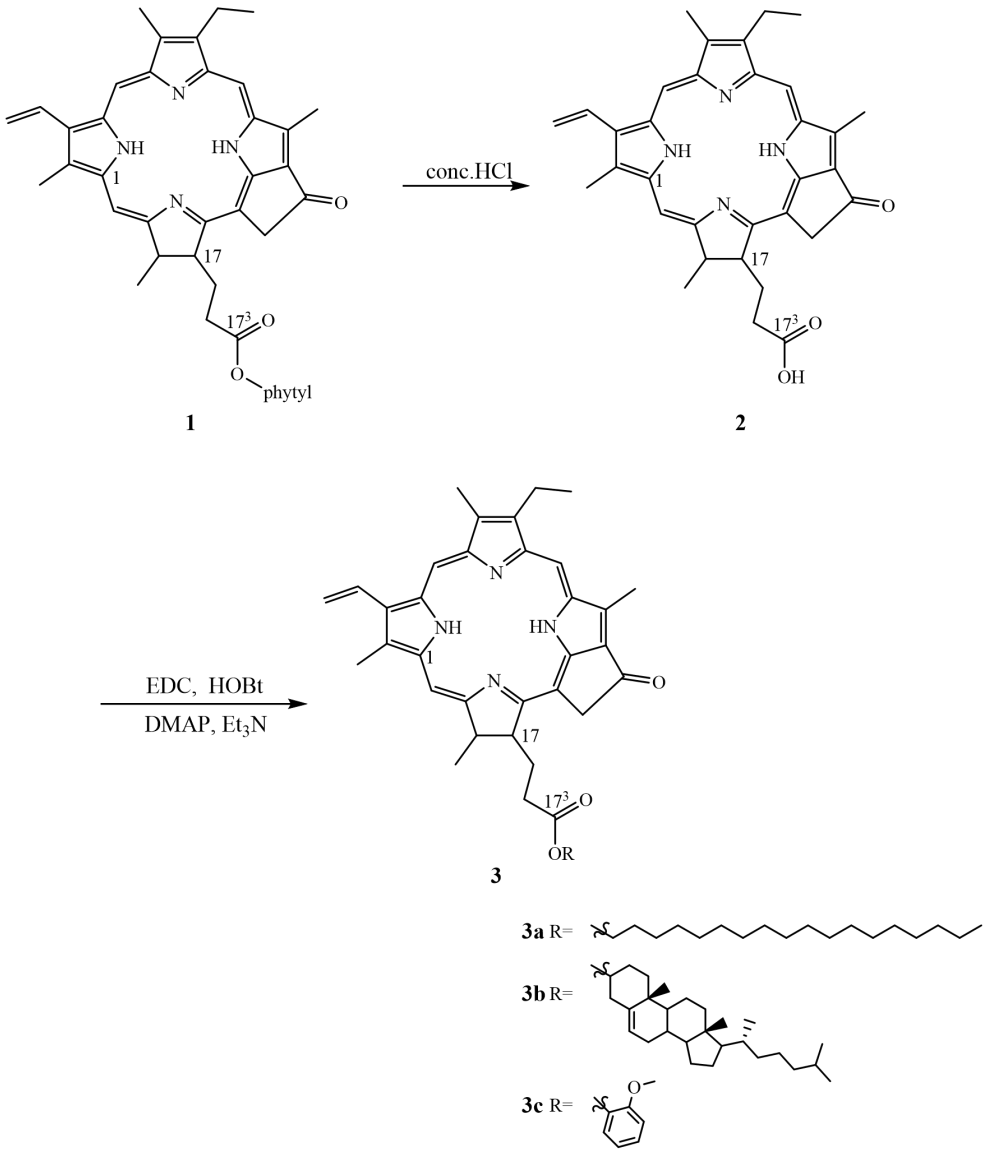

Scheme 1. Preparation scheme for pyropheophorbide *a* esters (**3a-c**).

2.1 Preparation of starting material

A sticky dark green chlorophyll tar (chlorophyll company, UK), which contains pyropheophytin *a* (**1**, Scheme 1) as the main identified component, was used as the starting material for the preparation of pyrophaeophorbide *a*. In order to obtain pure pyropheophytin *a* for use in the preparation, silica gel column chromatographic separation was performed, yielding 10 mg pure compound **1** from 2 g crude tar mixture after eluting with 528 ml eluent (hexane: ethyl acetate, 100: 1, 101 mL; 50:1, 102 mL; 20:1, 105 mL; 10:1, 220 mL). However, due to the low recovery (0.5%) and high consumption of organic solvent, this method was abandoned.

The derivative of compound **1,** pyropheophorbide *a* (**2**, Scheme 1), has been reported to be soluble in conc. HCl, dimethyl formamide, pyridine, and ammoniacal methanol (64). Among these solvents, conc. HCl was deemed to be the best as it plays dual roles: 1) hydrolysing compound **1** to form compound **2**; 2) providing a means to separate **2** from other impurities *via* the well-established method. By following the procedures reported by Li *et al.* (65) compound **2** was prepared successfully. The reaction (chlorophyll tar, 12 g) was carried out in a mixture of non-polar solvent diethyl ether (100 mL) and conc. HCl (250 mL). After the reaction was completed, the less polar impurities were concentrated in the upper, ether, phase, leaving compound **2** and other more polar components in the aqueous phase. In the second stage of separation the components in the aqueous (conc. HCl) phase were transferred to an organic solvent (dichloromethane, DCM) by dilution and extraction. This process was straightforward and, owing to the high yield of (**2**) compared with the yield of (**1**) obtained by chromatography (2.9% vs 0.5%), provided sufficient starting material for subsequent reactions.

2.2 Esterification

Esterification reactions of pyropheophorbide *a* with each of three different alcohols were achieved via the Steglich reaction using *N*-(3-dimethylaminopropyl)-*N*'-ethylcarbodiimide hydrochloride (EDC), the preferred member of the carbodiimide family for use as the coupling reagent in esterification reactions due to its simple handling practice (66). The mechanism of

carbodiimide-mediated esterification is shown in Figure 2.1.

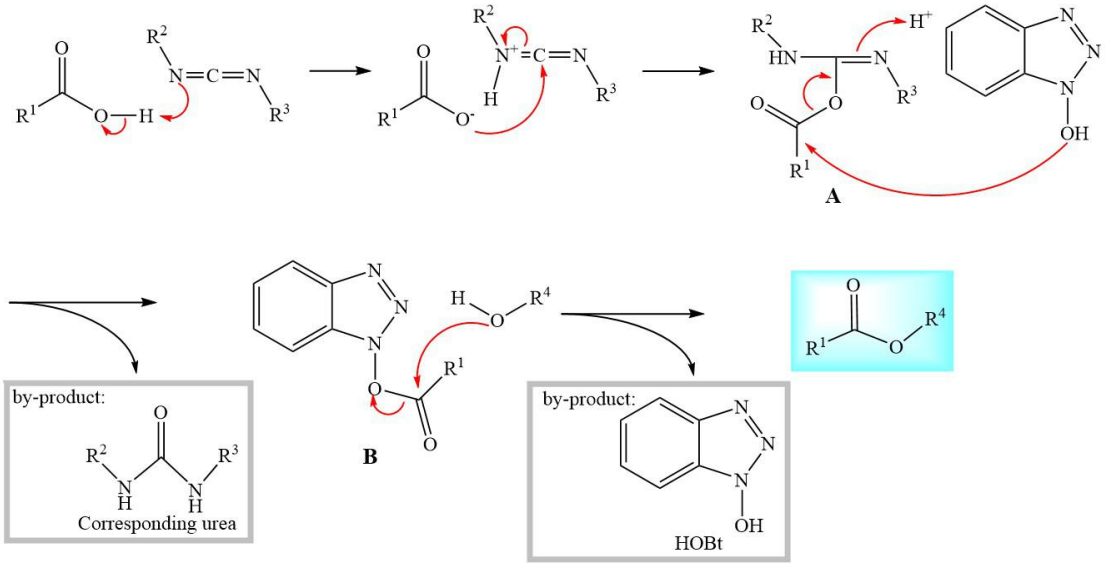

Figure 2.1 Mechanism of esterification with carbodiimide as the coupling reagent.

The carbodiimide active ester (**A,** Figure 2.1) is formed by nucleophilic attack of the carboxylate anion on the carbodiimide. With 1-hydroxybenzotriazole hydrate (HOBt) as an additive the active ester readily reacts to form the more stable HOBt ester (**B,** Figure 2.1), preventing a side reaction that results from rearrangement of the active ester to the *N*-acylisourea and which leads to reduction in yield of the ester (67). The formation of active ester is rapid while the second step, reaction with the alcohol, is rate-limiting (68). The second step was accelerated by the addition of *N,N*-dimethylpyridin-4-amine (DMAP) as the catalyst.

Neither strong base nor acid was used in this reaction, providing a mild environment for the substrates by comparison with typical esterification methods. The reaction was performed as a one-pot reaction and the resulting by-products and impurities were readily removed by extraction and column chromatography.

EDC is superior to dicyclohexylcarbodiimide (DCC), as it has a high solubility in water (200 g/L) and a wide range of organic solvents, so its urea by-product can be easily removed by extraction (69-71). By contrast, DCC and its by-product have similar soluble properties (72) with products and have to be removed by several filtration steps.

2.3 Analytical results

The structures of all synthesized compounds were confirmed through analysis of data obtained from proton nuclear magnetic resonance spectroscopy (^{1}H-NMR, Tables 2.1, 2.2) and electrospray ionization mass spectrometry (ESI-MS, Table 2.3). In addition, the derivatives (**3a-c**) of pyropheophorbide *a* were analyzed by UV-vis (Table 2.3), reversed phase-high performance liquid chromatography (RP-HPLC, Table 2.3) and electrospray ionization MS^n (ESI-MS^n, Figures 2.7, 2.11 and 2.12).

2.3.1 ^{1}H-NMR, UV-Vis spectrum, Mass spectrum and RP-HPLC

The protonated molecule obtained by ESI-MS of compound **2** is consistent with the calculated mass expected for the $[M+H]^+$ of pyrophaeophorbide *a* (Table 2.3). The ^{1}H-NMR and λ_{max} data are also consistent with that reported for **2** by Pallenberg, *et al.*(73) and Zheng, *et al.*(74), respectively. Given that compound **2** was prepared using a standard approach and that the analytical data are all consistent with that for the expected product it is reasonable to conclude that compound **2** is pyropheophorbide *a*. The ^{1}H-NMR spectrum of **2, 3a-c** are illustrated in Figures 2.2-2.5, respectively.

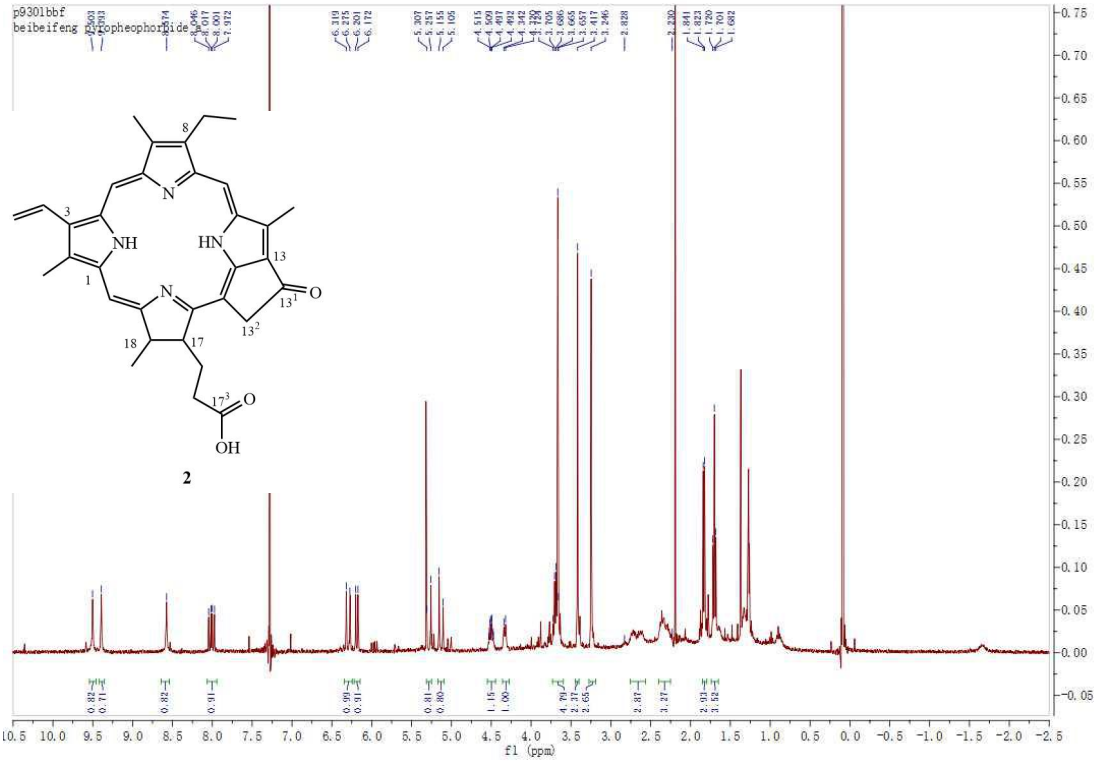

Figure 2.2 ^{1}H-NMR spectrum of **2**, the assignments for which are given in Tables 2.1and 2.2.

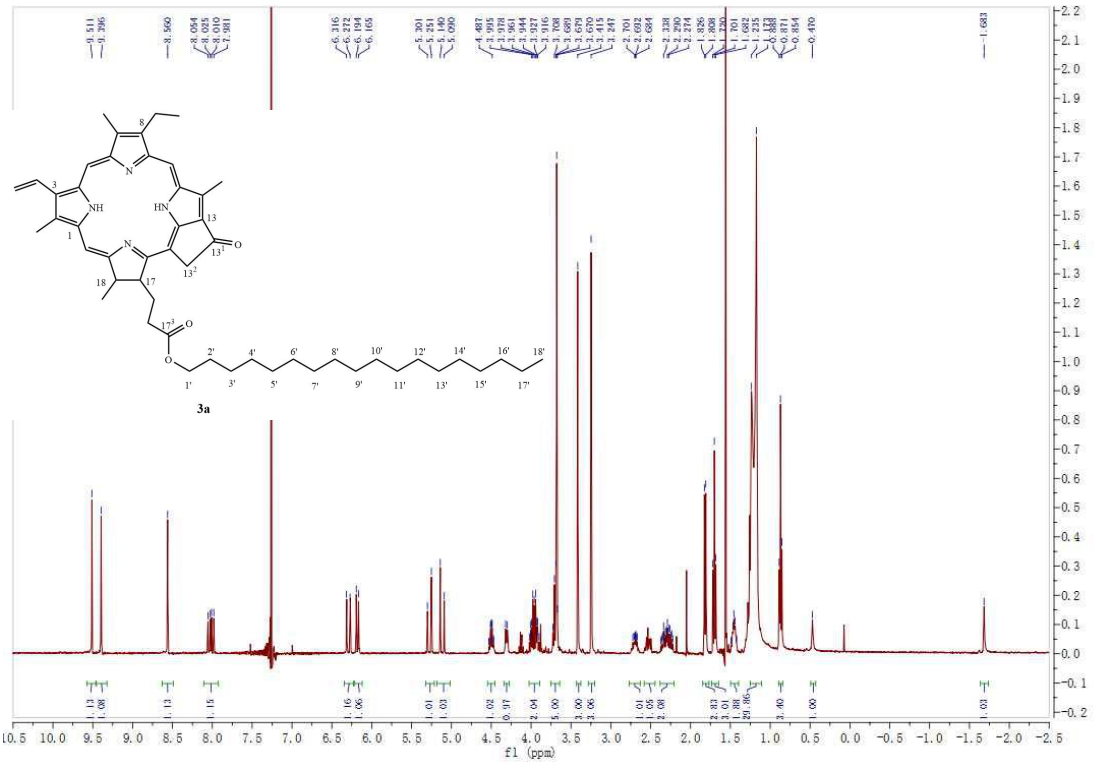

Figure 2.3 ^{1}H-NMR spectrum of **3a**, the assignments for which are given in Tables 2.1 and 2.2.

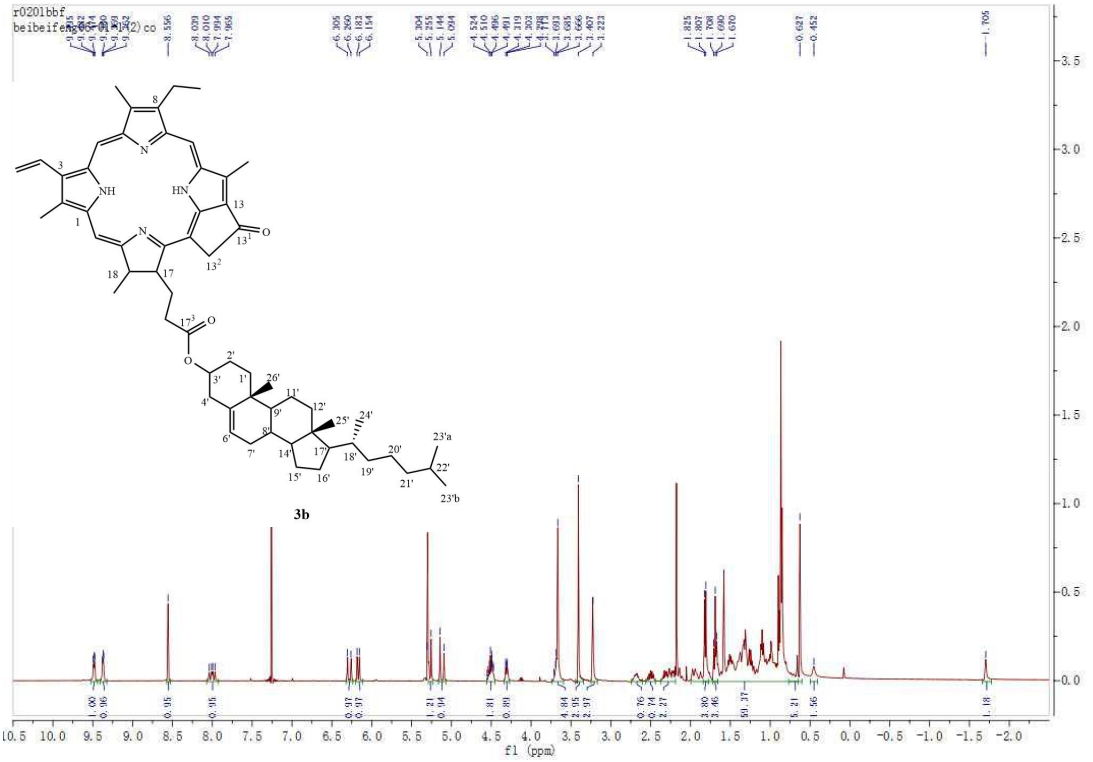

Figure 2.4 ^{1}H-NMR spectrum of **3b**, the assignments for which are given in Tables 2.1 and 2.2.

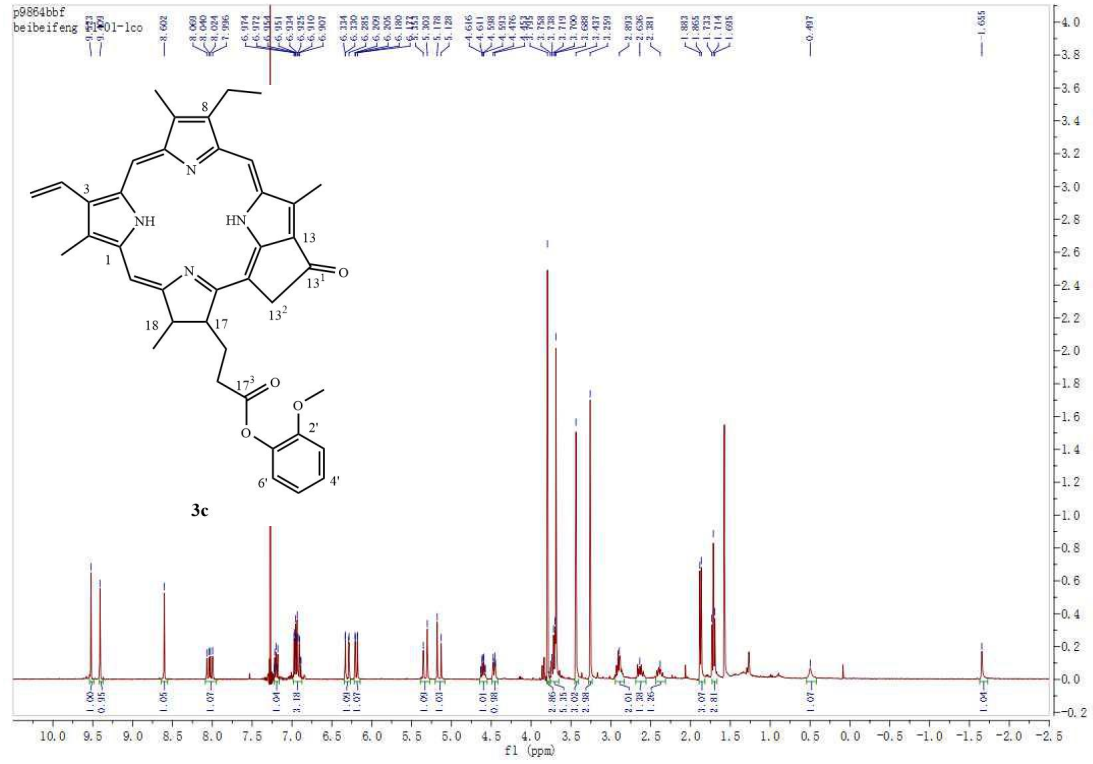

Figure 2.5 ^{1}H-NMR spectrum of **3c**, the assignments for which are given in Tables 2.1 and 2.2.

Table 2.1 ^{1}H-NMR data of the macrocycle in pyropheophorbide *a* (**2**) and its derivatives (**3a-c**) in $CDCl_3$.

	2	**3a**	**3b**	**3c**
5, 10, 20H (s, each 1H)	9.50, 9.39, 8.57	9.51, 9.40, 8.56	9.48 (t), 9.37 (t), 8.56	9.52, 9.41, 8.60
3^1-CH (dd, 1H)	8.01 (*J*=18.0 Hz, 11.6 Hz)	8.02 (*J*=11.6 Hz, 5.6 Hz)	7.99 (*J*=11.6 Hz, 6.4 Hz)	8.03 (*J*=11.6 Hz, 6.4 Hz)
3^2-CH_2 (d, each 1H)	6.30 (*J*=17.6 Hz), 6.19 (*J*=11.6 Hz)	6.29 (*J*=17.6 Hz), 6.18(*J*=11.6 Hz)	6.28 (J=18.0 Hz), 6.17 (J=11.6 Hz)	6.31 (*J*=18.0 Hz), 6.19 (*J*=11.6 Hz)
13^2-CH (exocyclic ring, d, 1H) 13^2-CH (exocyclic ring, d, 1H)	5.50 (*J*=20 Hz), 5.30 (*J*=20 Hz)	5.28 (*J*=20 Hz), 5.12 (*J*=20 Hz)	5.28 (*J*=20 Hz), 5.12 (*J*=20 Hz)	5.33 (*J*=20 Hz), 5.15 (*J*=20 Hz)
18H (dq, 1H)	4.50 (*J*=7.2 Hz, 2.0 Hz)	4.50 (*J*=7.2 Hz, 1.6 Hz)	4.51 (*J*=6.0 Hz, 2.0 Hz)	4.61 (*J*=7.2 Hz, 2.0 Hz)
17H (d, 1H)	4.33 (*J*=8.8 Hz)	4.31 (*J*=8.8 Hz)	4.31 (m)	4.46 (m)
8^1-CH_2 (q, 2H)	3.69 (*J*=7.6 Hz)	3.69 (*J*=7.6 Hz)	3.65 (m)	3.70 (*J*=7.6 Hz)
2^1,7^1, 12^1-CH_3 (ring CH_3, s, each 3H)	3.69, 3.42, 3.25	3.68, 3.42, 3.25	3.68, 3.41, 3.22	3.69, 3.44, 3.26
17^1-CH_2, 17^2-CH_2 (m, 4H)	2.83 – 2.23	2.80 – 2.20	2.80 – 2.20	2.90 – 2.35
18-CH_3 (d, 3H)	1.83 (*J*=7.2 Hz)	1.82 (*J*=7.2 Hz)	1.82 (*J*=7.2 Hz)	1.87 (*J*=7.2 Hz)
8^2-CH_3 (t, 3H)	1.70 (*J*=7.6 Hz)	1.70 (*J*=7.6 Hz)	1.69 (*J*=7.2 Hz, 8.0 Hz)	1.71 (*J*=7.6 Hz)
NH (s, 1H)	_	0.47, -1.68	0.45, -1.71	0.50, -1.66

Table 2.2 ^{1}H-NMR data of C-17^{3} side chain in pyropheophorbide *a* derivatives **(3a-c)** in $CDCl_3$.

	3a	**3b**	**3c**
1'-CH_2 (m, 2H)	3.96	_	_
2'-CH_2 (m, 2H)	1.44	_	_
3'-17'-CH_2 (m, 30H)	1.20	_	_
18'-CH_3 (t, 3H)	0.87 (*J*=6.8 Hz)	_	_
6'-CH (s, 1H)	_	5.30	_
3'-CH (m, 1H)	_	4.50	_
Other H* in cholesterol residue (m, 40H)	_	2.00 – 0.70	_
25'-CH_3 (s, 3H)	_	0.63	_
Benzene ring H (m, 4H)	_	_	7.20, 6.93
OCH_3 (s, 3H)	_	_	3.80

* Other H = 1',2',4',7',8',9',11',12',14',15',16',17',18',19',20',21',22',23'a,23'b,24',26' H

The protonated molecules obtained by ESI-MS of compounds **3a-c** are consistent with the calculated masses expected for the $[M+H]^+$ of the desired products and are the dominant ions in the spectra (Table 2.3), indicating success in their preparation, and good purity. Compounds **3a-c**, all show essentially the same chemical shift for each H resonance within the macrocycle as compound **2**. The resonances for the hydrogen atoms in the C-17^{3} ester side chain of **3a** gave integral intensities equating to two for the deshielded protons at δ = 3.96 and 35 hydrogens in the expected range between δ= 1.44 to 0.87. Similarly, the 3' proton in **3b** was identified at δ = 4.50, 40 alkyl hydrogens of the sterol in the range δ = 2.00 to 0.7 and the 6' alkene proton at δ = 5.29. Given its relative simplicity, the structure of **3c** could be fully assigned with the methoxyl protons at δ = 3.80 and the four aromatic protons at δ = 7.20 and 6.93. The analytical results are all consistent with the structures proposed for compounds **3a-c**, indicating their successful preparation *via* the reactions outlined in Scheme 1.

Table 2.3 UV-Vis, mass spectral and RP-HPLC data for **2** and its derivatives (**3a-c**).

	2	**3a**	**3b**	**3c**
Maximum absorption wavelength in methanol* (λ_{max}, nm)	665.1, 610.0, 539.9, 510.1, 410.0	665.1, 610.0, 539.9, 510.1, 410.0	665.1, 610.0, 539.9, 510.0, 410.0	665.1, 610.0, 539.9, 510.1, 410.0
Formula	$C_{33}H_{34}N_4O_3$	$C_{51}H_{70}N_4O_3$	$C_{60}H_{78}N_4O_3$	$C_{40}H_{40}N_4O_4$
Calculated mass	534.26	786.54	902.61	640.3
ESI-MS (*m/z* + 1)	535.2726	787.5508	903.6114	641.3151
Purity**	_	87.91%	88.77%	99.41%
Retention time***	_	15.9 min	16.0 min	10.2 min

* The scan range was from 330 to 800 nm. The measuring cuvette was 1 cm path length.
** The purity of **3a-c** was determined by its absorption percentage in the RP-HPLC/UV-vis spectrum at 665 ± 5 nm.
*** The retention time was obtained from the RP-HPLC/UV-vis chromatogram, the detail of which was described in Section 6.3.3.

The purity of the compounds is strongly suggested by the absence of additional and unattributable signals in the mass and ^{1}H-NMR spectra, as well as by the results of HPLC/UV-Vis analysis listed in Table 2.3. RP-HPLC employed an apolar (octadecyl-silica, ODS) stationary phase with moderately polar solvent (methanol and ethyl acetate) as mobile phase, so the compounds with shorter retention times represent those having highest polarity. Thus, **3a** and **3b**, which elute with similar retention times have similar polarity, while **3c** shows higher polarity. This result is consistent with that obtained from TLC for **3a-c** (R_f = 0.91, 0.91, 0.82, respectively, DCM: methanol 20:1 as the developing solvent).

Prowse *et al.* (75) and King *et al.* (76) reported the presence of a variety of sterol esters of chlorophyll derivatives in an ancient lake sediment and recent marine sediments as the degradation products of natural chlorophyll. Pyropheophobide *a* sterol esters were believed to be one of the components in some samples (75) after analysis by ^{1}H-NMR, GC-MS and HPLC. In this study, the high purity of compound **3b** illustrated from its RP-HPLC chromatogram (Figure 2.6) and the good yield (51.3%, Section 6.1.3), as well as its readily employed preparation procedure

demonstrates the feasibility of the approach for the efficient chemical synthesis of pyropheophorbide *a* cholesterol ester, which exists in many natural distributions. Hence, this prepared compound and its analogues could be used as standards in the confirmation of natural components in the future.

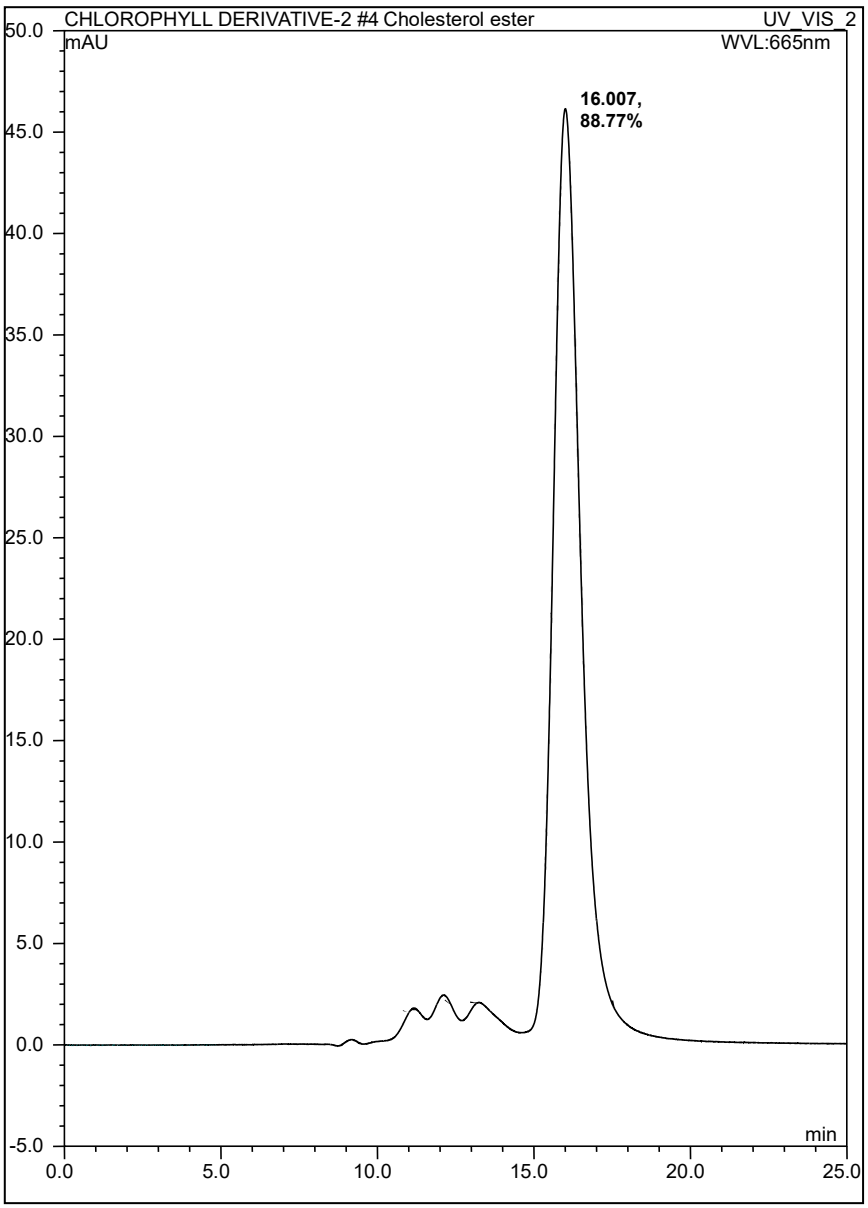

Figure 2.6 RP-HPLC of pyropheophorbide *a* cholesterol ester (**3b**) monitored by diode array detection and plotted at 665 nm.

2.3.2 ESI-MS^n

The multistage tandem mass spectra (MS^4) for compounds **3a-c** were recorded and are represented below in the form of dissociation maps which illustrate the losses of neutral species, the resulting product ions for each stage of MS^n and their relative

intensities (Figure 2.7, 2.11 and 2.12).

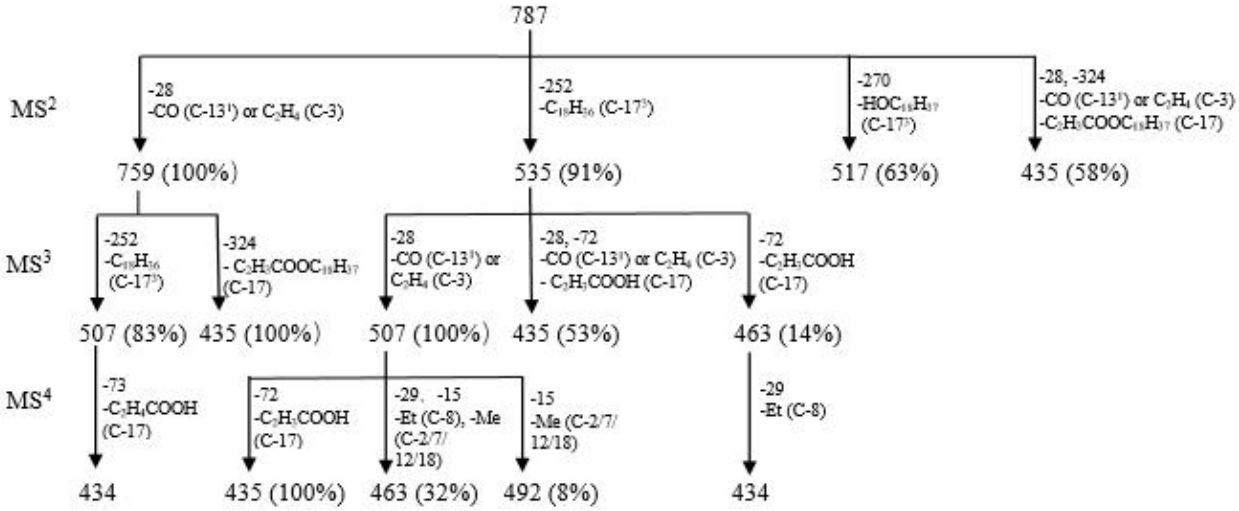

Figure 2.7 Dissociation map for pyropheophorbide *a* derivative **3a** obtained using its multistage tandem mass spectra data and detailing losses with the corresponding relative intensities.

In the MS^2 stage for compound **3a**, loss of the carbonyl group on C-13^1 or C_2H_4 on C-3 (*m/z* 28), $C_{18}H_{36}$ on C-17^3 (*m/z* 252), the 1-octadecanol on C-17^3 (*m/z* 270) and both the fragment of *m/z* 28 and the ester chain on C-17 (*m/z* 324) gave ion *m/z* 759, 535, 517 and 435 from $[M + H]^+$ (*m/z* 787), respectively. The first one (*m/z* 759) was the predominant fragment ion. As demonstrated in the literature by Chillier *et al.* (77), the loss of neutral species of *m/z* 324 involves the hydrogen and electron migration within the C-17 side chain. The assortment of structural information for this process is illustrated in Figure 2.8.

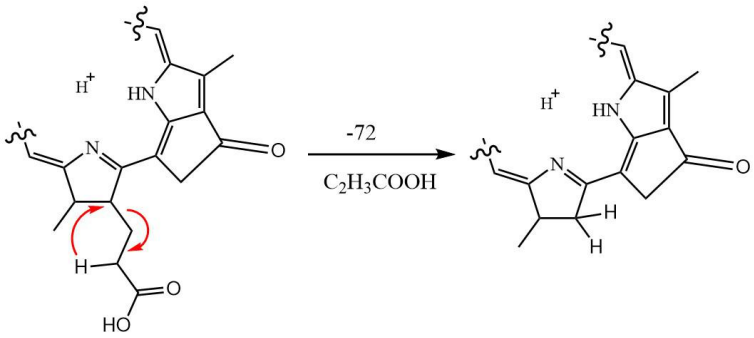

Figure 2.8 Mechanism for the product ion formation arising from loss of 72 in the tandem mass spectrum for pyropheophrbide *a* derivatives.

In MS^3, either the carbonyl group on C-13^1 or the substituent on C-17 or C-17^3 was lost, resulting in the formation of product ions at *m/z* 507, 463 and 435. This was

followed by the further losses of the residue on C-17 and also the radical ion from methyl/ethyl group on the macrocycle in the next stage.

This dissociation pattern was consistent with that reported by Chillier *et al.* (77) and Moulin *et al.* (78) In Moulin's report, protoporphyrin IX (Figure 2.9) showed losses of *m/z* 59 and *m/z* 73 in the electrospray ionization tandem mass spectrum (EI-MS^2), identified as losses of one acetate group and one propionate group, respectively (Figure 2.10).

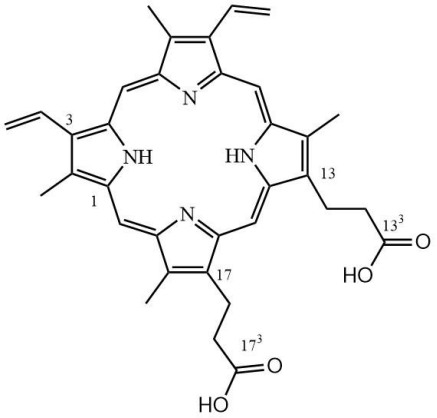

Figure 2.9 Protoporphyrin IX

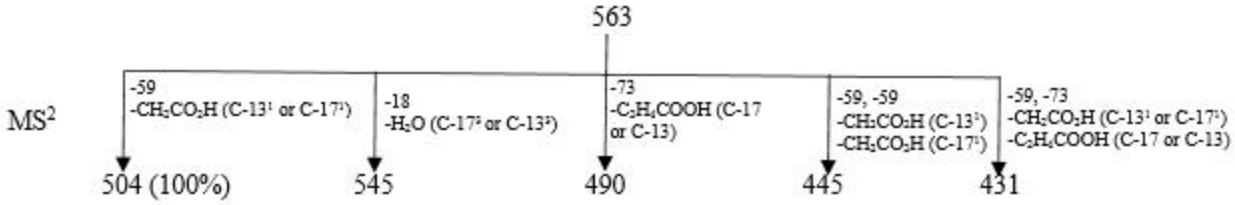

Figure 2.10 EI-MS^2 for protonated protoporphyrin IX.

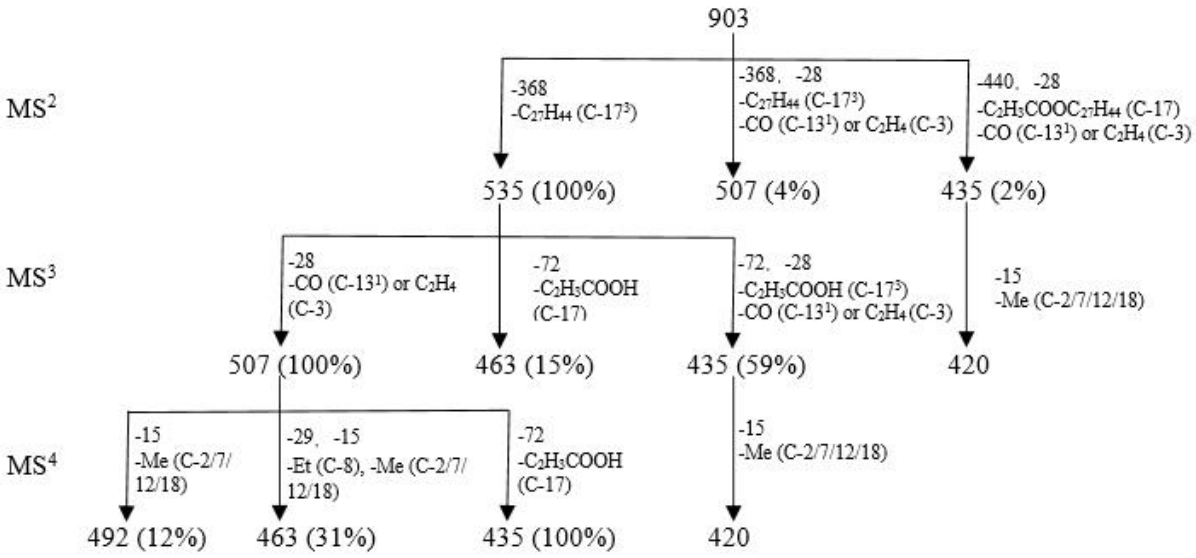

Figure 2.11 Dissociation map for pyropheophorbide *a* derivative **3b** obtained using its multistage mass spectral data and detailing losses with the corresponding relative intensities.

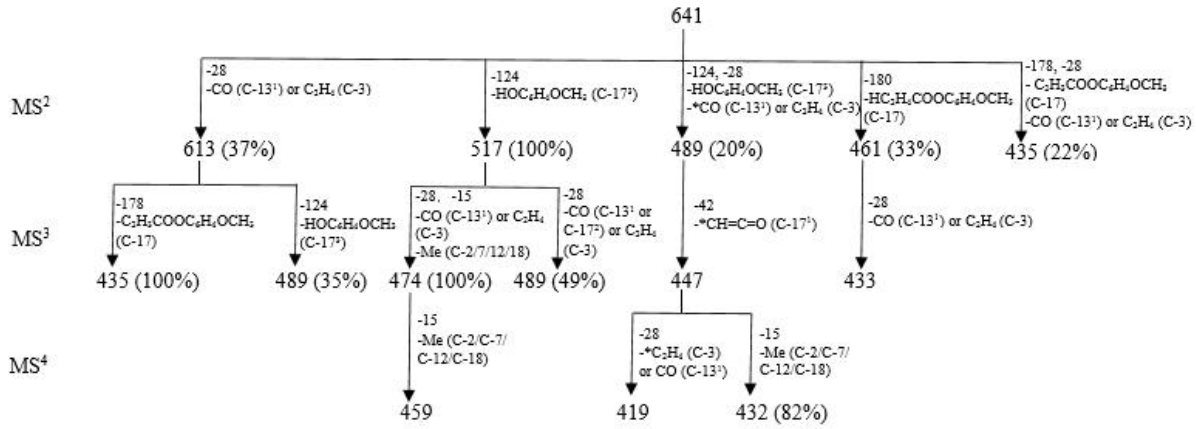

Figure 2.12 Dissociation map for pyropheophorbide *a* derivative **3c** obtained using its multistage tandem mass spectra data and detailing losses with the corresponding relative intensities. *There is another possibility for the loss of 28, 42 and 28 in this sequence, the detail of which is stated in text (Page 43).

The tandem mass spectra of compounds **3b** and **3c** show generally identical patterns in terms of the neutral losses with that of **3a**. To be specific, the cleavages occurred at four main positions, C-13[1] or C-3 and C-17 as well as C-17[3] followed by the losses of radical ions from the methyl and ethyl groups. Consideration of the order of the losses in the dissociation pathways for these compounds indicates that the radical species generally occur later than the other losses, which is consistent with the previous report by Wilson *et al.* (79). For example, in the sequence *m/z* 787→535→507→463 of **3a** (Figure 2.7), *m/z* 903→535→507→463 of **3b** (Figure 2.11) and *m/z* 641→517→474→459 of **3c** (Figure 2.12), the losses of methyl/ethyl groups appeared in the last stage. This indicates that the pathway is diagnostic for

the pyropheophorbide *a* esters (79).

The most intense MS^2 product ion for **3b** was *m/z* 535 (loss of $C_{27}H_{44}$, Figure 2.11). The greater abundance of the ion than for the corresponding product ions from **3a** (most intense product ion: *m/z* 759) and **3c** (most intense product ion: *m/z* 517) indicates that the cholesterol ester bond is the less stable among the three components. Notably, the stability difference is also reflected in the stability in acid media where hydrolysis of the ester occurred for the cholesteryl derivative but not for **3a** or **3c** (Section 3.4). Moreover, the most intense MS^2 product ion at *m/z* 517 for **3c** was generated as the result of cleavage of the alkyl oxygen bond, and appeared with 63% intensity for **3a** (MS^2, Figure 2.7) but was not observed at all for **3b**. The formation of the ion can be rationalized as resulting from hydrogen transfer *via* the conjugation system of aromatic ring (Figure 2.13).

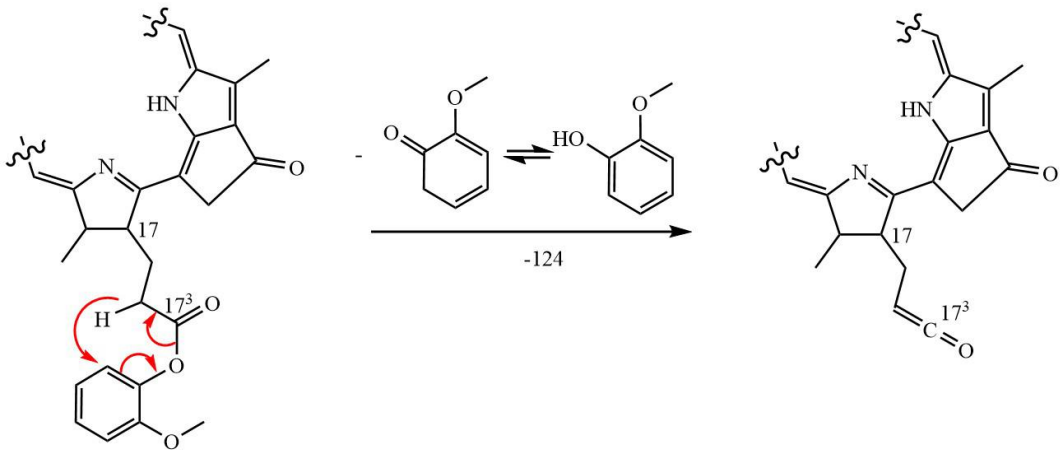

Figure 2.13 Suggested mechanism for the loss of *m/z* 124 in the MS^2 for **3c**.

The dissociation behavior of compound **3c** differs from that of the two related compounds **3a** and **3b** in the loss of 42 from *m/z* 489 to give *m/z* 447 during MS^3. There are two possibilities for this: 1) the loss of ketene (CH_2=C=O, *m/z* 42) is from C-17^1 as shown in Figure 2.12; 2) the loss of the substituent CH=CH_2 (*m/z* 27) from C-3 together with any one of the methyl groups (*m/z* 15) on the macrocycle, thus the loss of *m/z* 28 before and after this stage of dissociation would be C=O either on C-13^1 or on C-17^2. The extra hydrogen for the C_2H_4 on C-3 could have come from the macrocycle *via* hydrogen migration.

2.4 Summary

This chapter has reported the preparation and characterization of three pyropheophorbide *a* esters (**3a-c**). As expected, they showed similar properties in terms of maximum absorption in UV-vis spectrum due to the shared macrocycle structure which is responsible for the spectrum pattern. Similarly, because of the structural difference on C-17[3] side chain, differences were observed in their MS^n dissociation pathways (Section 2.3.2).

Moreover, the achievement in synthesizing various esters with high purity demonstrates the potential for the future for making a wide range of ester derivatives of pyropheophorbide *a.*

3. Triglycine derivatives of pyropheophorbide *a* esters

In Section 1.2.2 (2), it was reported that HPPH, a pyropheoporbide *a* derivative, has already entered into clinical trial as a promising PS candidate. Its high absorption in the preferred range 650 - 850 nm (ε_{max} ~47,000 at 665 nm) encouraged scientists developing novel PSs derived from the pyropheoporbide *a* family.

Inspired by HPPH, modification on C-3[1] of pyropheophorbide *a* esters was carried out. The vinyl group on C-3 was converted to a 1-hydroxyl ethyl substituent, followed by esterification with triglycine. The relation between localization preference and the structure of the photosensitizer has been reviewed in Section 1.4, so introducing the triglycine group in **3a-c** could be expected to give the resulting compounds amphiphilic properties. Hence, the solubility comparison between these two series (**3a-c** and **6a**/**6c**) will be able to provide some basic idea in future research *in vitro* or *vivo*.

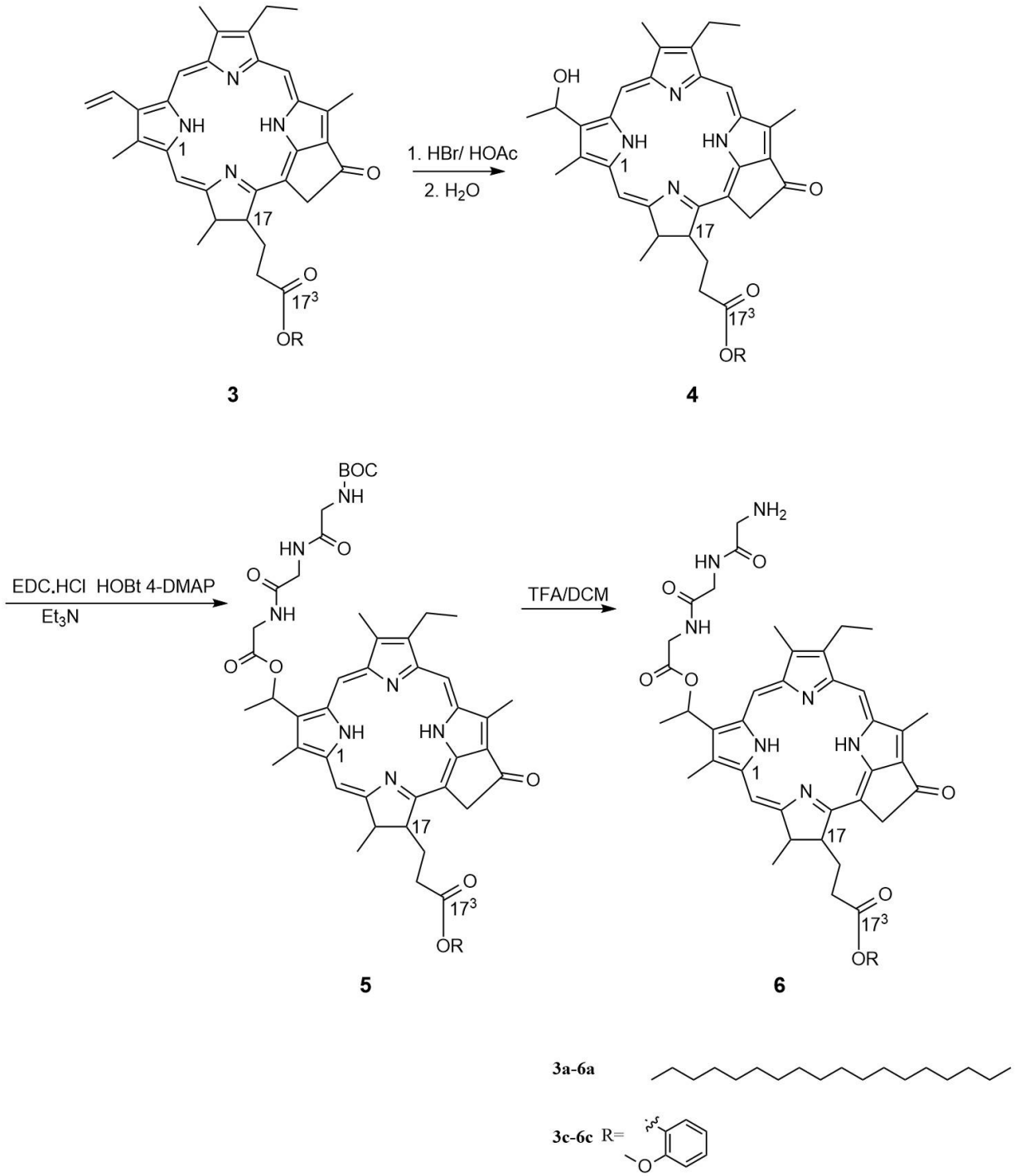

Scheme 2. Preparation scheme for the triglycine derivative of 3-(1-hydroxyethyl) pyropheophorbide *a* esters (**6a**, **6c**).

3.1 Preparation of the 3-(1-hydroxyethyl) pyropheophorbide *a* esters (4a and 4c, Scheme 2)

Compound **3** was converted to **4** via two steps: 1) addition of hydrogen bromide to the 3-vinyl group, resulting in the formation of the 3-(1-bromoethyl) group; 2) treatment

of the 3-(1-bromoethyl) group with H_2O to obtain the 3-(1-hydroxyethyl) substituent. The possible mechanism for these steps is shown in Figure 3.1.

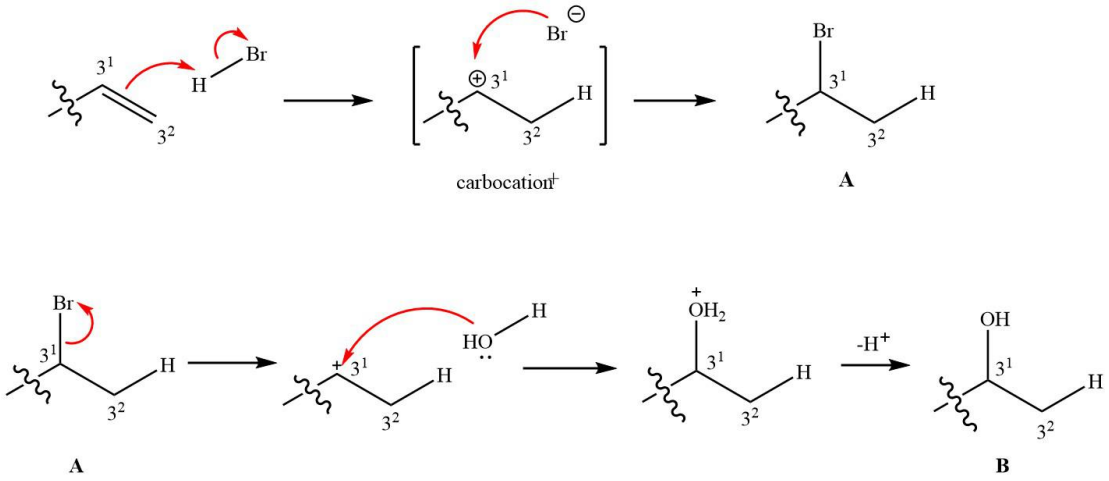

Figure 3.1 Schematic diagram representing the mechanism for HBr addition to a chlorin vinyl group, and subsequent hydrolysis.

The carbocation preferentially forms on the secondary carbon (C-3^1, Figure 3.1) instead of the primary carbon (C-3^2, Figure 3.1) as the former is more stable, so the halide (Br) group is attached at the C-3^1, more alkyl-substituted carbon (Markovnikov's rule), resulting in the C-3^1-bromoalkyl derivative (**A**, Figure 3.1). The bromine group was rapidly, 0.5 h in this case, substituted by hydroxyl group (**B**, Figure 3.1) once H_2O was introduced into the system.

3.2 Preparation of the Boc-triglycine derivatives of 3-(1-hydroxyethyl) pyropheophorbide *a* esters (5a and 5c, Scheme 2)

Compounds **5a** and **5c** were prepared *via* the Steglich esterification reaction, the mechanism of which was elaborated in Section 2.2. The proportion of the acid to the alcohol was changed from 1: 2 to 1.5: 1 in order to consume the alcohol (obtained from the last step) as much as possible.

3.3 Preparation of the triglycine derivatives of 3-(1-hydroxyethyl) pyropheophorbide a esters (6a and 6c, Scheme 2)

Either dilute aqueous HCl solution (1-2 M) or trifluoroacetic acid (TFA) solution (20% in DCM) is widely employed as the agent for Boc deprotection. The latter was used in this case in order to simplify the subsequent workup. Thus, only neutralization was needed before column purification, removing the possibility of product loss during the extraction procedure that would be required with aqueous HCl.

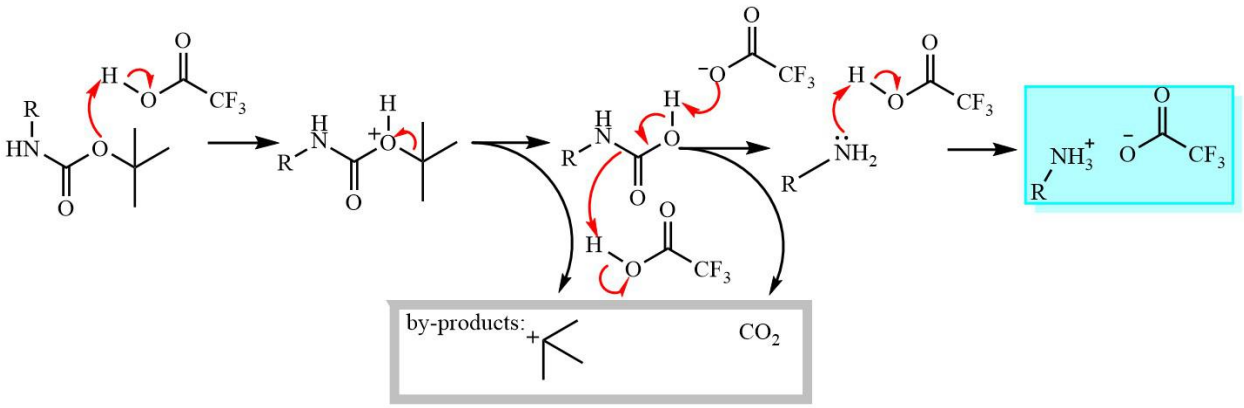

Figure 3.2 Schematic diagram representing the mechanism for Boc deprotection.

Figure 3.2 shows the mechanism for the Boc deprotection of alkyl amine. Boc-protected alkyl amine becomes protonated, the hydrogen being donated by TFA, followed by the loss of *t*-butyl cation. The TFA salt of the amine is formed after releasing one molecule of CO_2 from the carbamic acid under the acidic conditions. Free amine (compounds **6a, 6c**) was obtained by the addition of triethylamine (Et_3N) to the salt complex.

3.4 Preparation of the triglycine derivatives of 3-(1-hydroxyethyl) pyropheophorbide *a* cholesterol ester (12, Schemes 3, 4)

Triglycine derivatives of 3-(1-hydroxyethyl) pyropheophorbide *a* 1-octadecanol ester, **6a,** and 2-methoxyl phenol ester, **6c,** were obtained *via* Scheme 2. However, the same preparation protocol was attempted but failed for the preparation of 3-(1-hydroxyethyl) pyropheophorbide *a* cholesterol ester (**12**, Schemes 3, 4). The

C-17^3 ester bond was found to be hydrolysed in the presence of HBr solution (33% wt. in acetic acid), which either did not occur or was negligible in the preparation for compounds **4a** and **4c**.

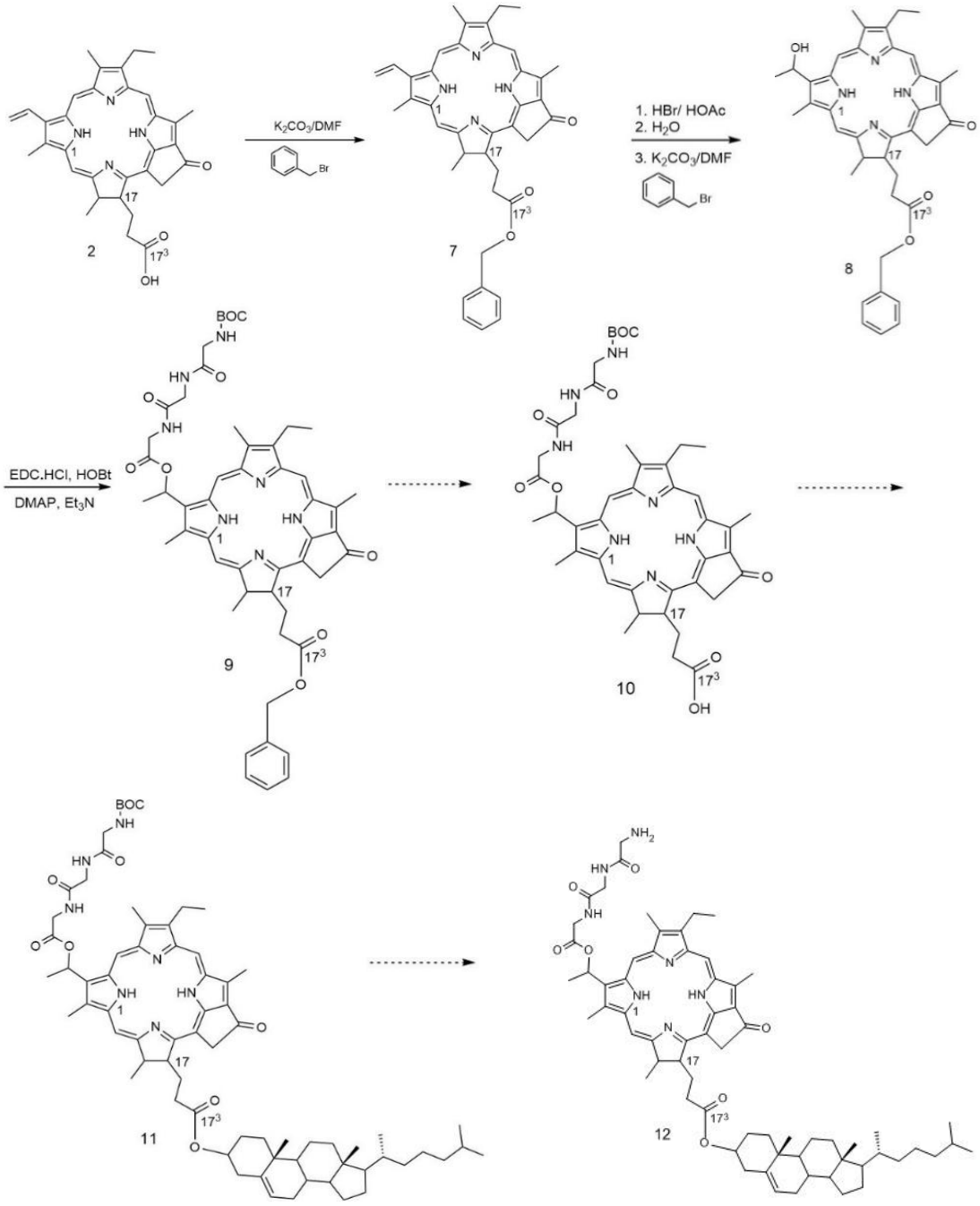

Scheme 3. Preparation scheme for the triglycine derivative of 3-(1-hydroxyethyl) pyropheophorbide *a* cholesterol ester (**12**).

An alternative method to the formation of **12** was designed using pyropheophorbide *a* (**2**, Scheme 3) as the starting material. The C-17^3 acid residue was protected by a benzyl group (**7**, Scheme 3), which was considered more likely to be stable in the acid

environment during the next step. This proved incorrect, the benzyl group being removed during the formation of the bromine product. Hence, the benzyl group was re-introduced after the vinyl substituent on C-3 was converted to the C-3^1-hydroxyethyl group (**8**, Scheme 3), and compound **8** was reacted to form the ester bond with *N*-(tert-butoxycarbonyl) triglycine (Boc-Gly-Gly-Gly-OH, **9**, Scheme 3) *via* the Steglich esterification.

The removal of the benzyl protecting group was attempted *via* catalytic hydrogenation using 10% palladium on carbon (Pd-C) as the catalyst and hydrogen as the gas source (filled balloon). The reaction was performed at room temperature (25 ± 2 ℃), and in a variety of solvents (listed in Table 3.1). The proportion of Pd-C to the substrate (**9**, Scheme 3) was increased from 0.2: 1 to 0.3: 1 and again to 0.4: 1. All of the corresponding results are reported in Table 3.1.

Table 3.1 Details of reaction conditions for attempts at the preparation of compound **12**.

Attempted times	Solvent	Pd-C proportion to substrate, reaction time	MS Result
1	Ethanol	0.2: 1 for 16 hours	Substrate remains, no target at expected *m/z* value
2	Methanol	0.2: 1 for 16 hours	Substrate remains, no target at expected *m/z* value
3	Methanol: THF: H_2O_2: 1: 0.2	0.2: 1 for 16 hours, then 0.3: 1 for 4 hours	Target appeared at expected *m/z* value, but could not be reproduced
4	Methanol: THF: H_2O_2: 1: 0.2	0.4: 1 for 4 hours	Expected *m/z* value for compound **16** (Figure 3.3)

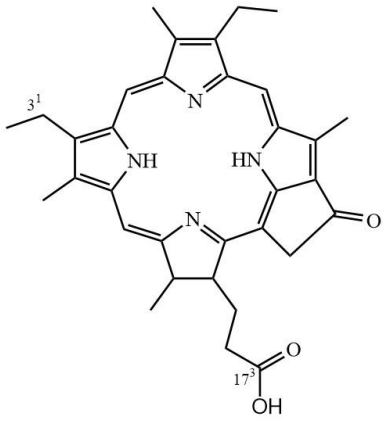

Figure 3.3 3-Ethyl pyropheophorbide *a* acid (**16**).

Although the correct *m/z* for the target compound was observed in the analytical results from reaction 3 (Table 3.1), the reproducibility of the reaction was so poor that the positive result was not observed in repeated reactions. Considering that the Pd-C was most likely to be saturated by the substrate, leading to the loss of its activity, the proportion of Pd-C was increased to 40% (reaction 4, Table 3.1). The result of this reaction showed that the C-O bond at the C-3^1 position was broken alongside the removal of the benzyl protecting group, resulting in the formation of 3-ethyl pyropheophorbide *a* (compound **16**, suggested from the mass spectrum).

In summary, the Pd-C catalytic hydrogenation failed in the deprotection of the benzyl group, therefore another route (Scheme 4) for the formation of compound **12** was designed as follows.

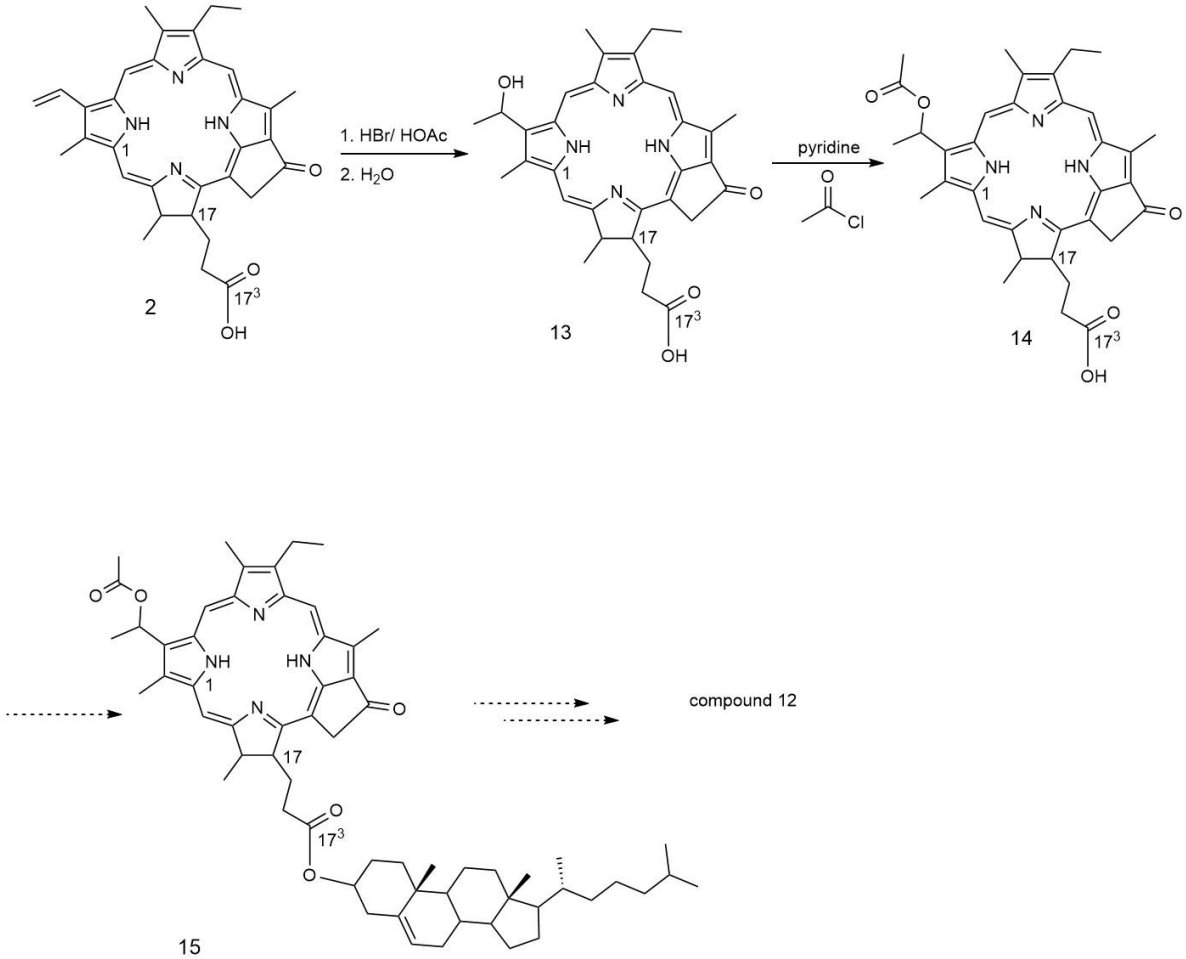

Scheme 4. Alternative scheme of the preparation for the triglycine derivative of 3-(1-hydroxyethyl) pyropheophorbide *a* cholesterol ester (**12**).

With compound **2** as the starting material, the vinyl substituent on C-3 was converted to the C-3[1]-hydroxyethyl group (compound **13**, Scheme 4) during the first step of the third scheme. The hydroxyl residue was then protected by an acetyl group (compound **14**, Scheme 4).

Although DCC and the combination of EDC and HOBt, or EDC and *N*-hydroxysuccinimide (NHS) were used as the coupling agents, respectively, for Steglich reaction, no ion corresponding to compound **15** could be observed on the mass spectrum.

3.5 Analytical results

The structures of all synthesized compounds were confirmed through analysing data from ESI-MS and ^{1}H-NMR spectroscopy. In addition, the derivatives of -pyropheophorbide *a,* **6a** and **6c,** were analyzed by UV-vis, RP-HPLC and ESI-MS^{n}.

3.5.1 ^{1}H-NMR, UV-Vis spectrum, MS and RP-HPLC

The ESI-MS spectra of compounds **4a-6a** and **4c-6c** gave protonated molecules ($[M+H]^{+}$) that are consistent with the calculated masses expected for the corresponding pyrophaeophorbide *a* derivatives (Tables 3.6 and 3.7). ^{1}H-NMR spectrums of **4a-6a** and **4c-6c** are illustrated in Figure 3.4-3.6 and Figure 3.7-3.9, respectively.

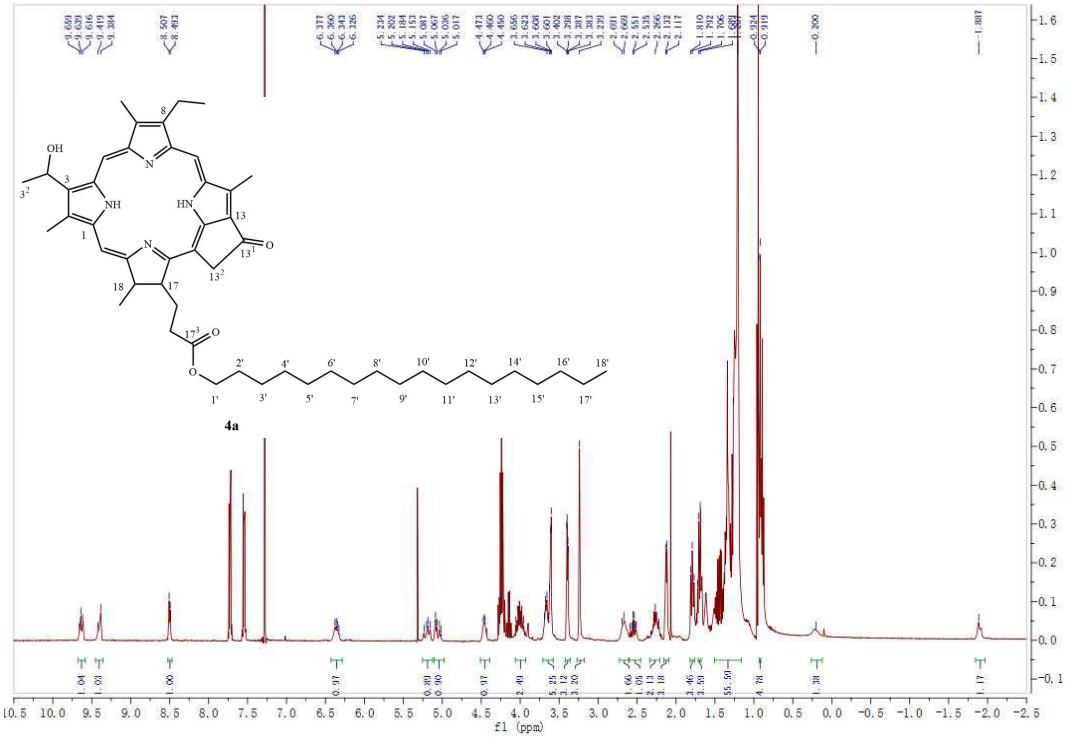

Figure 3.4 ^{1}H-NMR spectrum of **4a**, the assignments for which are detailed in Tables 3.2 and 3.3.

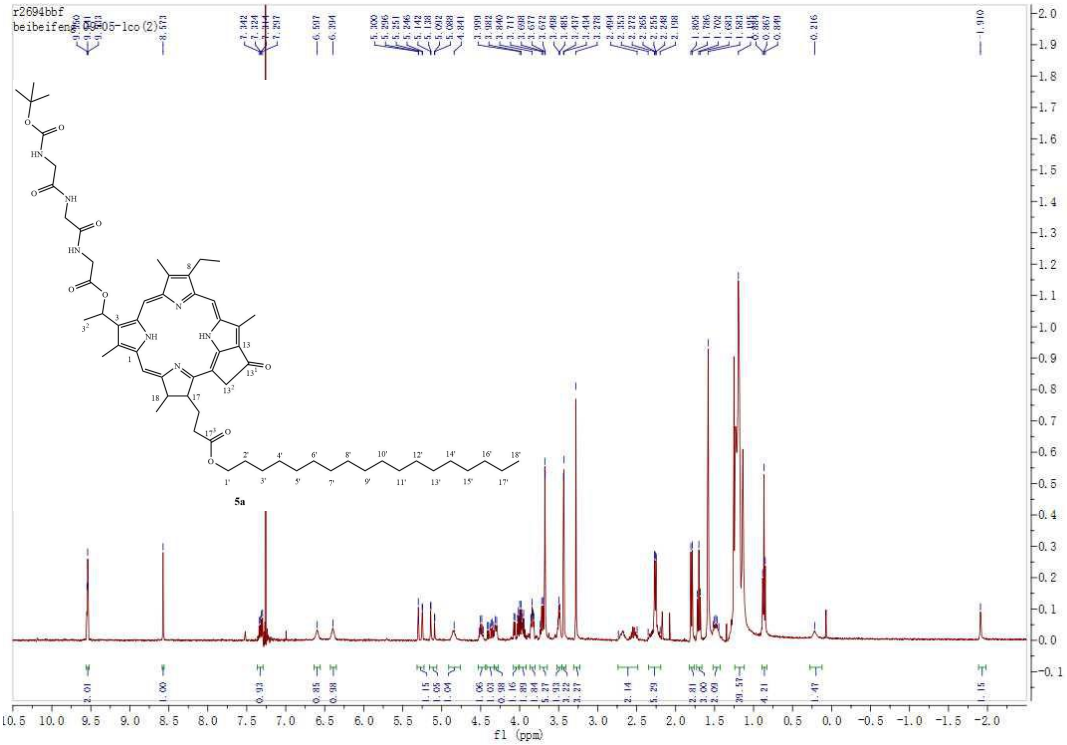

Figure 3.5 ^{1}H-NMR spectrum of **5a**, the assignments for which are detailed in Tables 3.2 and 3.3.

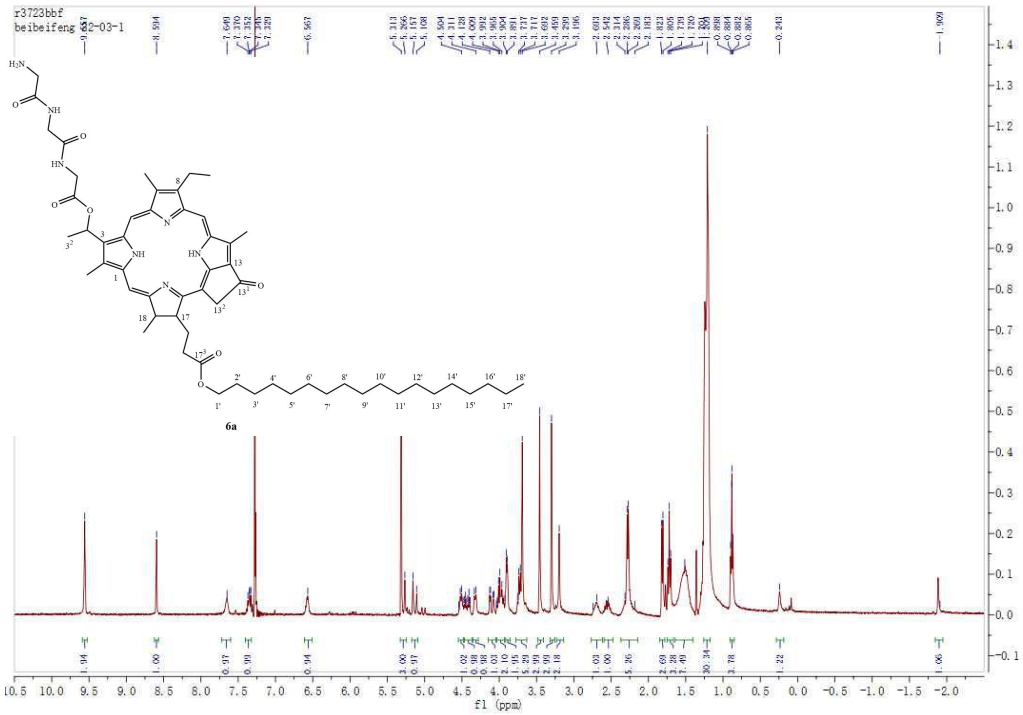

Figure 3.6 ^{1}H-NMR spectrum of **6a**, the assignments for which are detailed in Tables 3.2 and 3.3.

The modification of compounds **3a** and **3c** to produce **4a**-**6a** and **4c**-**6c**, centered exclusively on the C-3 position. The protons of the other substituents on the macrocycle ring show essentially identical chemical shifts, especially within the ester chain on the C-17^{3}, indicating that the structural modifications made at the C-3 position do not significantly alter the conjugation within the aromatic ring.

Table 3.2 ^{1}H-NMR data of the macrocycle in pyropheophorbide *a* derivatives (**4a-6a**) in $CDCl_3$.

	4a	**5a**	**6a**
5, 10, 20H (s, 1H)	9.64 (t), 9.38 (d), 8.51(d)	9.54 (t, 2H, *J*=3.6 Hz), 8.57	9.56, 9.54, 8.59
3^1-CH (q, 1H)	6.35 (*J*=6.8 Hz)	7.31 (*J*=7.2 Hz)	7.35 (*J*=7.2 Hz)
13^2-CH_2 (exocyclic ring, dd, each 1H)	5.19 (*J*=12.8, 7.2 Hz), 5.05 (*J*=12.4, 8.0 Hz)	5.27 (*J*=1.6, 18.0 Hz), 5.11 (*J*=1.6, 18.4 Hz)	5.29 (d, *J*=18.8 Hz), 5.13 (d, *J*=19.6 Hz)
18H (1H)	4.46 (m)	4.49 (q, *J*=7.6 Hz)	5.51 (q, *J*=8.0 Hz)
17H (1H)	4.01 (m, merged with 1'-CH_2)	4.29, 4.31 (d, *J*=7.2 Hz)	4.33, 4.31 (d, *J*=9.2 Hz)
8^1-CH_2 (q, 2H)	3.66 (*J*=7.2 Hz)	3.72 (*J*=7.6 Hz)	3.72 (*J*=8.0 Hz)
2^1,7^1, 12^1-CH_3 (ring CH_3, s, each 3H)	3.61 (m), 3.39 (m), 3.24 (s)	3.67, 3.44, 3.28	3.69, 3.46, 3.30
17^1-CH_2, 17^2-CH_2 (m, 4H)	2.69-2.22	2.73-2.20	2.74-2.18
3^2-CH_3 (d, 3H)	2.12 (*J*=6.0 Hz)	2.26 (dd, J=2.8, 4.0 Hz)	2.28 (J=6.8 Hz)
18-CH_3 (d, 3H)	1.79 (t, *J*=7.2, 9.6 Hz)	1.79 (*J*=7.6 Hz)	1.81 (*J*=7.2 Hz)
8^2-CH_3 (t, 3H)	1.71 (*J*=6.4 Hz)	1.70 (*J*=7.6 Hz)	1.72 (*J*=7.6 Hz)
NH (s, each 1H)	0.2, -1.89	0.22, -1.91	0.24, -1.91

Table 3.3 ^{1}H-NMR data of the C-17[3] and C-3[1] side chains in **4a-6a** in $CDCl_3$.

	4a	**5a**	**6a**
1'-CH_2 (m, 2H)	4.01	3.97	4.01
2'-CH_2 (m, 2H)	1.44	1.48	1.51
3'-17'-CH_2 (m, 30H)	1.20	_	1.21
3'-17'-CH_2 (m, 30H) and Boc group(9H)	_	1.20	_
18'-CH_3 (t, 3H)	0.87 (*J*=6.8 Hz)	0.87 (*J*=6.8 Hz)	0.82 (*J*=6.8 Hz)
NH (s, 1H) in Boc protected triglycine residue	_	6.60, 6.39, 4.84	7.65, 6,57
NH_2 (s, 2H) in triglycine residue	_	_	1.51
CH_2 (m,6H) in (Boc protected) triglycine residue	_	4.38 (m, 1H), 4.04 (dd, *J*=4.8, 14.0 Hz, 1H) 3.84 (m, 2H), 3.50 (t, 2H, *J*=7.2 Hz)	4.43 (m, 1H), 4.10 (dd, 1H, *J*=4.8, 13.6 Hz), 3.90 (d, 2H, *J*=5.2 Hz), 3.20 (s, 2H)

The change in the chemical shift of protons on C-3 substituent from high (δ = 8.02, 6.29 for **3a**; δ = 8.03, 6.19 for **3c**) to low frequency (δ = 6.35, 2.12 for **4a**; δ = 6.42, 2.14 for **4c**) is consistent with the vinyl group being substituted by the 1-hydroxyethyl group as expected. Moreover, the resonances for the hydrogen atoms of the C-3 side chain of **4a** (**4c**) gave integral intensities equaling to one proton at δ = 6.35 (6.42) and three protons at δ = 2.12 (2.14), which also confirms the expected conversion on C-3.

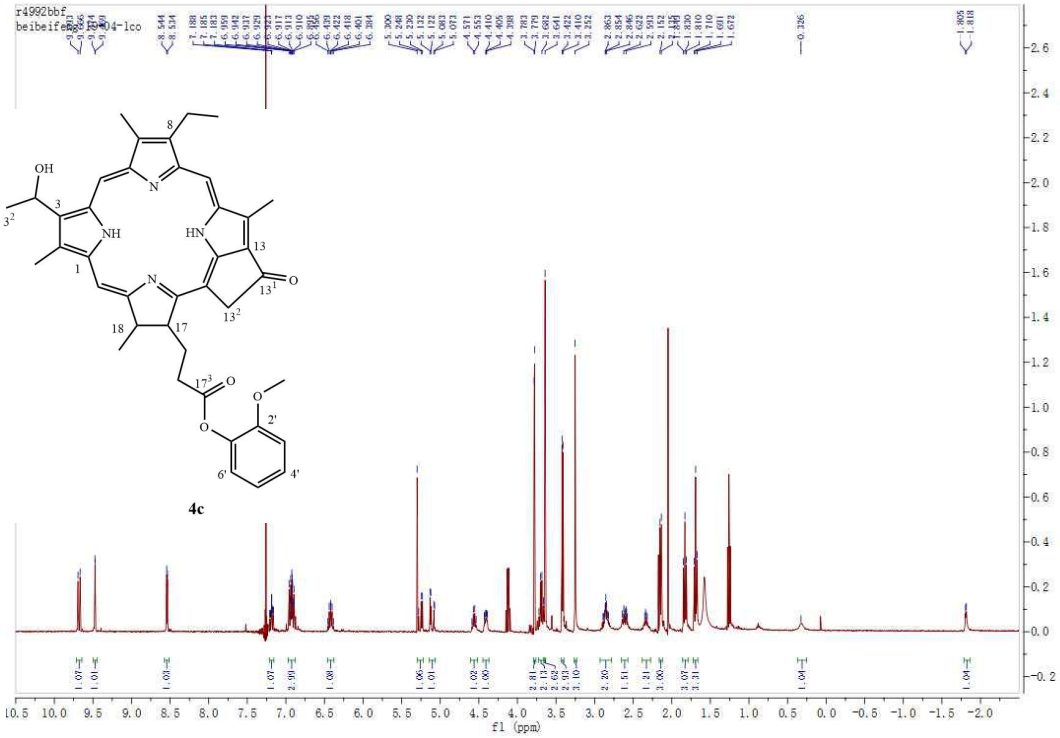

Figure 3.7 ^{1}H-NMR spectrum of **4c**, the assignments for which are detailed in Tables 3.4 and 3.5.

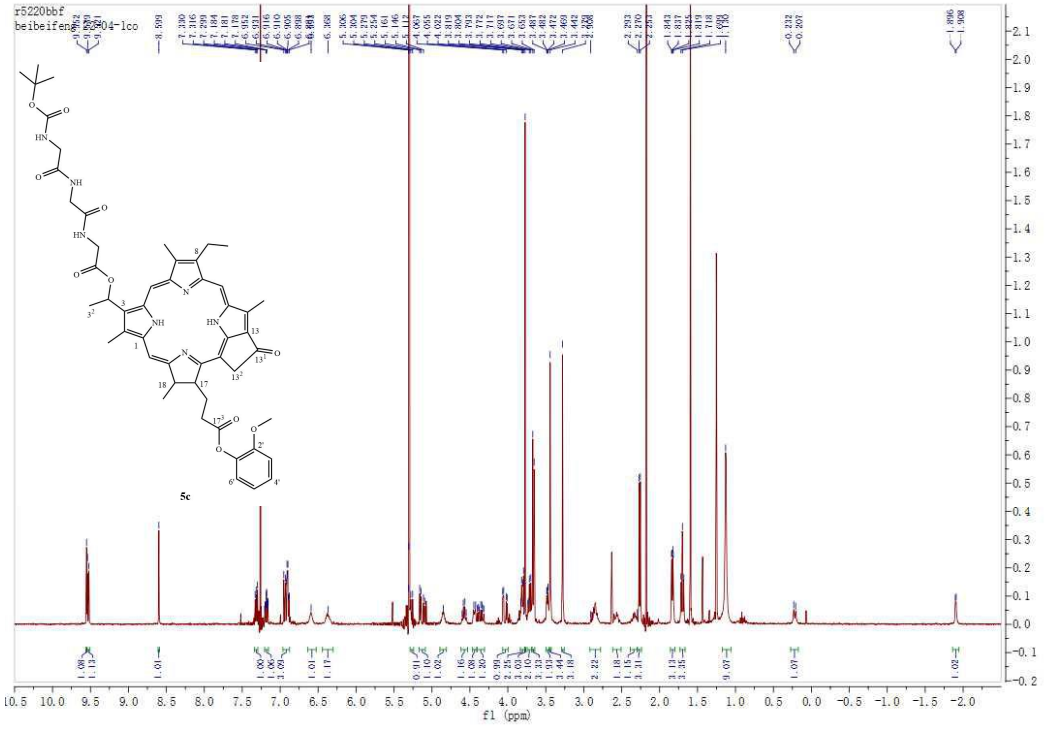

Figure 3.8 ^{1}H-NMR spectrum of **5c**, the assignments for which are detailed in Tables 3.4 and 3.5.

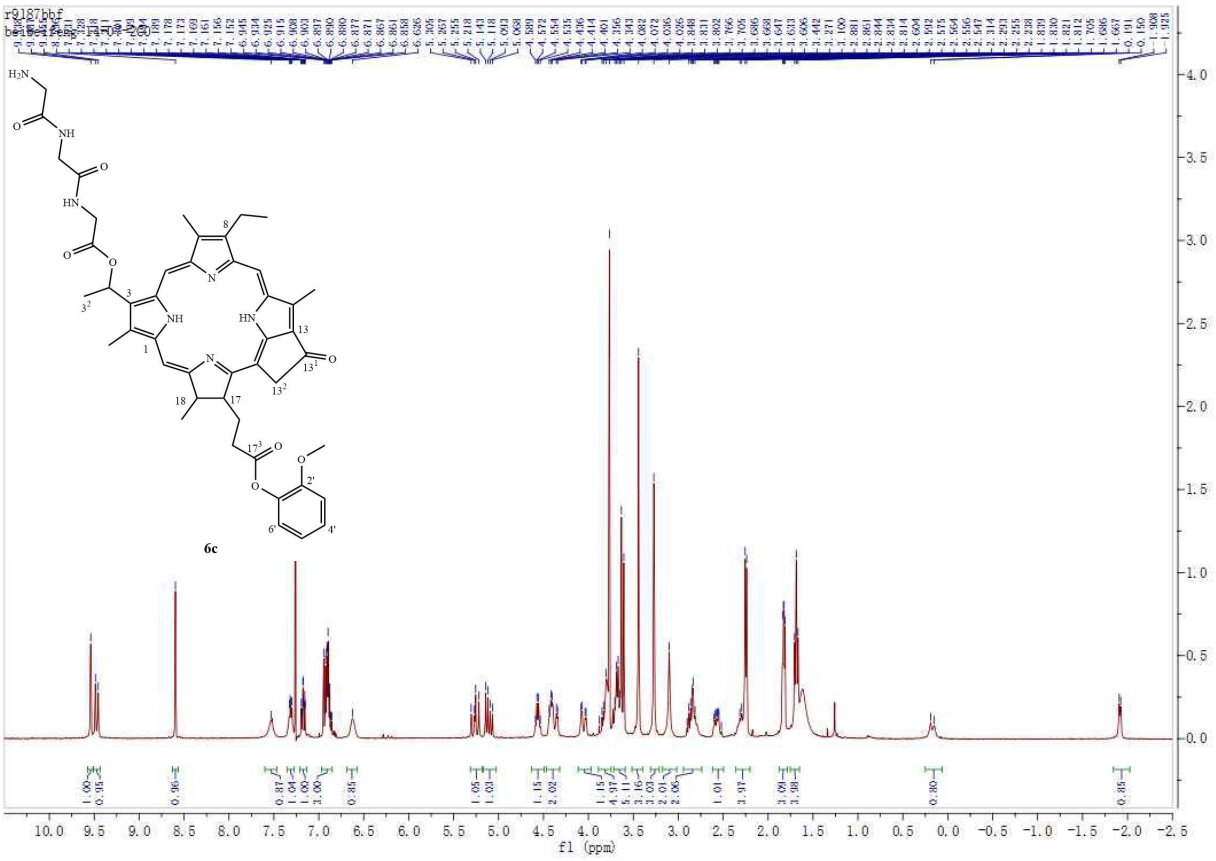

Figure 3.9 ^{1}H-NMR spectrum of **6c**, the assignments for which are detailed in Tables 3.4 and 3.5.

Table 3.4 ^{1}H-NMR data of the macrocycle in **4c-6c** in $CDCl_3$.

	4c	**5c**	**6c**
5, 10, 20H (1H)	9.68 (d, *J*=9.8 Hz), 9.47 (d, *J*=2.0 Hz), 8.54 (d, *J*=4.0 Hz)	9.55 (s), 9.53 (d, *J*=7.2 Hz), 8.60 (s)	9.54 (s), 9.47 (d, *J*=12.8 Hz), 8.60 (s)
3^{1}-CH (1H)	6.42 (m)	7.32 (q, *J*=5.6, 0.8 Hz)	7.31 (q, *J*=4.0, 2.8 Hz)
13^{2}-CH_2 (exocyclic ring, dd, 2H)	5.26 (1H, *J*=12.8, 7.2 Hz), 5.10 (1H, *J*=15.6, 4.0 Hz)	5.27 (1H, *J*=6.4, 3.6 Hz), 5.12 (1H, *J*=15.6, 4.0 Hz)	5.26 (1H, *J*=15.2, 4.8 Hz), 5.12 (1H, *J*=10 Hz)
18H (1H)	4.56 (d, *J*=7.2 Hz)	4.56 (q, *J*=8.4 Hz)	4.56 (q, *J*=7.0Hz)
17H (1H)	4.41 (m)	4.44 (m)	4.05 (dd, *J*=4.0, 14.4 Hz)
8^{1}-CH_2 (2H)	3.69 (q, *J*=7.6 Hz)	3.72 (m)	3.67 (m)
2^{1},7^{1}, 12^{1}-CH_3 (ring CH_3, each 3H)	3.64 (s), 3.42 (d, *J*=74.8 Hz), 3.25 (s)	3.66 (d, *J*=7.2 Hz), 3.44 (s), 3.28 (s)	3.62 (d, *J*=10.8 Hz), 3.44 (s), 3.27 (s)
17^{1}-CH_2, 17^{2}-CH_2 (m, 4H)	2.89-2.32	2.91-2.29	2.90-2.29
3^{2}-CH_3 (d, 3H)	2.14 (*J*=6.8 Hz)	2.26 (*J*=6.8 Hz)	2.24 (d, *J*=6.8)
18-CH_3 (3H)	1.83 (t, *J*=7.6 Hz)	1.83 (d, *J*=4.8 Hz)	1.83 (q, *J*=3.6 Hz)
8^{2}-CH_3 (t, 3H)	1.69 (t, *J*=7.6 Hz)	1.70 (t, *J*=7.6 Hz)	1.69 (t, *J*=7.6 Hz)
NH (each s, 1H)	0.33, -1.81 (d, *J*=5.2 Hz)	0.21 (d, *J*=10.0 Hz), -1.90 (d, *J*=4.8 Hz)	0.17 (d, *J*=15.6 Hz), -1.91 (d, *J*=6.8 Hz)

The chemical shifts and the integral intensities at δ = 4.38 (1H), 4.04 (1H) 3.84 (2H), 3.50 (2H) and at δ = 4.36 (1H), 4.04 (1H), 3.81 (2H), 3.48 (2H) in the ^{1}H-NMR spectra of **5a** and **5c**, respectively, were identified to belong to the three methylene groups (CH_2) in triglycine, hence confirming the formation of the ester bond between **4a**/**4c** and triglycine. Likewise, 9 protons of the Boc group and three protons on NH

groups were also identified at δ = 1.20 (**5a**), δ = 1.13 (**5c**) and δ = 6.60, 6.39, 4.84 (**5a**), δ = 6.59, 6.37, 4.85(**5c**), respectively.

Table 3.5 ^{1}H-NMR data of the C-17[3] and C-3[1] side chains in **4c-6c** in $CDCl_3$.

	4c	**5c**	**6c**
Benzene ring H (m,4H)	7.19 (1H), 6.92 (3H)	7.18 (1H), 6.90 (3H)	7.17 (1H), 6.90 (3H)
OCH_3 (s,3H)	3.78 (d, *J*=1.6 Hz)	3.77	3.77
Boc group (9H)	—	1.13	—
NH (s,1H) in Boc protected triglycine residue	—	6.59, 6.37, 4.85	7.53, 6.63
NH_2 (s, 2H) in triglycine residue	–	–	1.61
CH_2 (m,6H) in (Boc protected) triglycine residue	—	4.36 (m, 1H), 4.04 (dd, *J*=4.8, 13.2 Hz, 1H), 3.81 (m, 2H), 3.48 (m, 2H)	4.41 (m, 2H), 3.83 (m, 2H), 3.10 (s, 2H)

Similarly, the proton signals of Boc group disappeared in the deprotected compounds **6a** and **6c** while those of the methylene and NH groups were found at δ = 7.65, 6.57(**6a**), δ =7.53, 6.63 (**6c**) and δ = 4.43 (1H), 4.10 (1H), 3.90 (2H), 3.20 (2H) (**6a**), δ = 4.41 (2H), 3.83 (2H), 3.10 (2H) (**6c**), respectively, as expected. Although the integral intensities of peaks at δ = 1.51/1.61 do not equal to two protons, it is reasonable to assign part of them to protons on NH_2 group for **6a**/**6c**, considering the fact that the exchangeable NH_2 signals become more likely to coalesce with the water

signal brought into the system *via* the deuteriated solvent or the substances themselves.

Table 3.6 UV-Vis, mass spectral and RP-HPLC data for **4a-6a**.

	4a	**5a**	**6a**
Maximum absorption wavelength in Methanol* (λ_{max}, nm)	660.1, 605.0, 534.9, 505.0, 405.1	660.1, 605.0, 534.9, 505.0, 405.1	660.0, 605.0, 535.0, 505.0, 405.1
Formula	$C_{51}H_{72}N_4O_4$	$C_{62}H_{89}N_7O_9$	$C_{57}H_{81}N_7O_7$
Calculated mass	804.56	1075.67	975.62
ESI-MS (*m/z* + 1)	805.5649	1076.6802	976.6283
Purity**	—	—	94.2%
Retention time***	–	–	8.2 min

* The scan range was from 330 to 800 nm. The measuring cuvette was of path length 1 cm.
** The purity of **4a-6a** was manifested by its peak area percentage in the RP-HPLC/UV-Vis chromatogram at 660 nm.
*** The retention time was obtained from the RP-HPLC/UV-vis chromatogram, the detail of which was described in Section 6.3.3.

Table 3.7 UV-Vis, mass spectral and RP-HPLC data for **4c-6c**.

	4c	**5c**	**6c**
Maximum absorption wavelength in methanol* (λ_{max}, nm)	660.1, 605.0, 534.9, 505.0, 405.1	660.1, 605.0, 534.9, 505.0, 405.1	660.0, 605.0, 535.0, 505.0, 405.1
Formula	$C_{40}H_{42}N_4O_5$	$C_{51}H_{39}N_7O_{10}$	$C_{46}H_{51}N_7O_8$
Calculated mass	658.32	929.43	829.38
ESI-MS (m/z + 1)	659.3245	930.4388	830.3883
Purity**	—	—	91.5%
Retention time***	–	–	5.6 min

* The scan range was from 330 to 800 nm. The measuring cuvette was 1 cm wide.
** The purity of **4c-6c** was manifested by its absorption percentage in the RP-HPLC/UV-Vis spectrum at 660 nm.
*** The retention time was obtained from the RP-HPLC/UV-vis chromatogram, the detail of which was described in Section 6.3.3.

Comparing with **3a-c**, the maximum absorption wavelengths of **6a** and **6c** in the red range demonstrate a blue-shift from 665 nm (Table 2.3) to 660 nm (Table 3.6 and 3.7). This is believed to be related to the saturation of the double bond on C-3, resulting in a small reduction in the extent of conjugation in the macrocycle system, since the intermediates **4a**, **4c** and **5a**, **5c** all show maximum absorption at the identical wavelength (Table 3.6, 3.7).

As described in Section 2.3.1, the shorter the retention time is, the higher the polarity of the compounds. Thus, **6c**, having the shorter retention time has higher polarity than **6a**, and the TLC (DCM: methanol 20:1 as the developing solvent) results gave the same indication as their R_f values equal 0.05 and 0.1, respectively.

3.5.2 ESI-MS^n

The multistage tandem mass spectrometry (MS^5) for compounds **6a** and **6c** was recorded and dissociation maps illustrating the losses of neutral species, the resulting product ions and their relative intensities were produced for each stage (Figures 3.10 and 3.12).

The loss of the triglycine substituent (189 Da) in MS^2 of **6a** and **6c** gave rise to the only detected MS^2 product ion at *m/z* 787 and 641, respectively. It is formed by hydrogen migration, most likely from the methyl group on C-3^2 (80), a mechanism for which is suggested in Figure 3.11. Chen *et al*. (81) in 2016 reported a similar loss from 2-(1-hexyloxyethyl)-2-devinyl pyropheophorbide (HPPH, MS = 636) in MS^2, involving loss of neutral *n*-hexanol (MS = 102) from $[M + H]^+$ = 637 to give *m/z* 535. The following stages of MS^n showed identical dissociation pathways as those for compound **3a/3c**. The losses of neutral species on C-3/13/17 occur prior to those of radicals from the methyl/ethyl group on C-7/8.

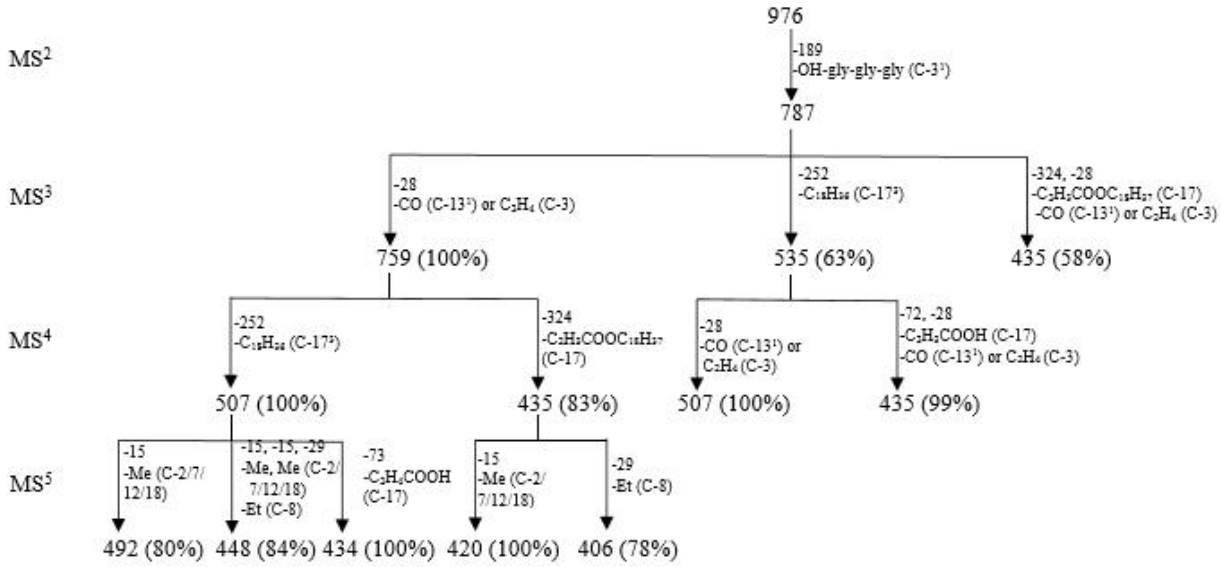

Figure 3.10 Dissociation map for pyropheophorbide *a* derivative **6a** obtained using its multistage tandem mass spectra data and detailing losses with the corresponding relative intensities.

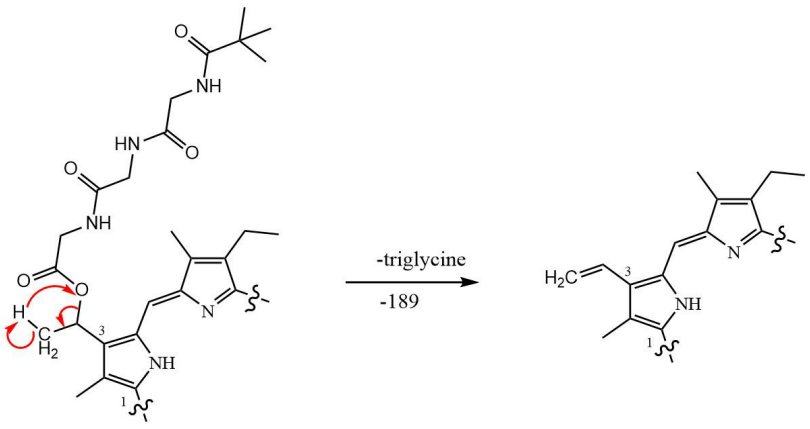

Figure 3.11 Assortment of structural information for the formation and loss of *m/z* 189 in multistage tandem mass spectrum for pyropheophrbide *a* derivatives.

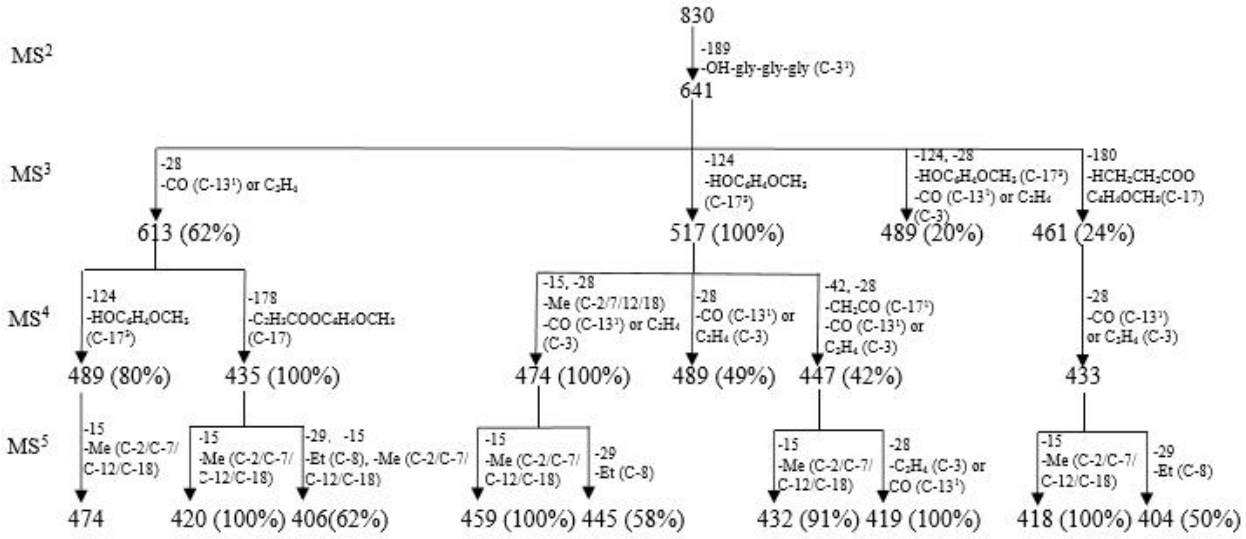

Figure 3.12 Dissociation map for pyropheophorbide *a* derivative **6c** obtained using its multistage tandem mass spectra data and detailing losses with the corresponding relative intensities.

3.6 Summary

This chapter has reported the preparation and characterization of triglycine derivatives (**6a** and **6c**) of pyropheophorbide *a* esters **3a** and **3c**. As expected, they showed blue shift for maximum absorption in UV-vis spectrum due to the reduction in the extent of the conjugated system between the vinyl group and the macrocycle, but still meet the wavelength requirement for ideal PS.

For the MS^n dissociation pathway, the loss first occurred from the ester bond of the C-3^1 for both components, followed by the similar loss of species with corresponding precusors **3a** and **3c**, respectively.

The successful modification on both C-17^3 and C-3^1 expanded the family of pyropheophorbide derivatives as promising PDT candidates, which meanwhile, provided references and guideline to relevant research in the future.

The solubility and polarity study among these prepared compounds **3a-c**, **6a** and **6c** will be discussed and elaborated in following Chapter 4.

4. Solubility and polarity

4.1 Solubility measurement of 3a-c

Six sequential concentrations of each of compounds **3a-c** were prepared in methanol and the corresponding UV-Vis absorptions at 665.1 nm were recorded (Table 4.1). The standard response curves for each component were plotted and the equation for the line of best fit and R^2 values were determined (Figures 4.1-4.3).

Table 4.1 UV-Vis absorption of **3a-c** in sequential concentrations under 665 nm.

Compound	Concentration in methanol (mg/ 100 mL)	Absorption
3a	10	1.878
	6	1.137
	4	0.782
	2	0.411
	1	0.217
	0.5	0.108
3b	10	0.688
	7.5	0.587
	5	0.483
	2	0.206
	1	0.106
	0.5	0.055
3c	7.4	1.797
	3.7	1.001
	1.85	0.645
	0.925	0.351
	0.4625	0.181
	0.222	0.088

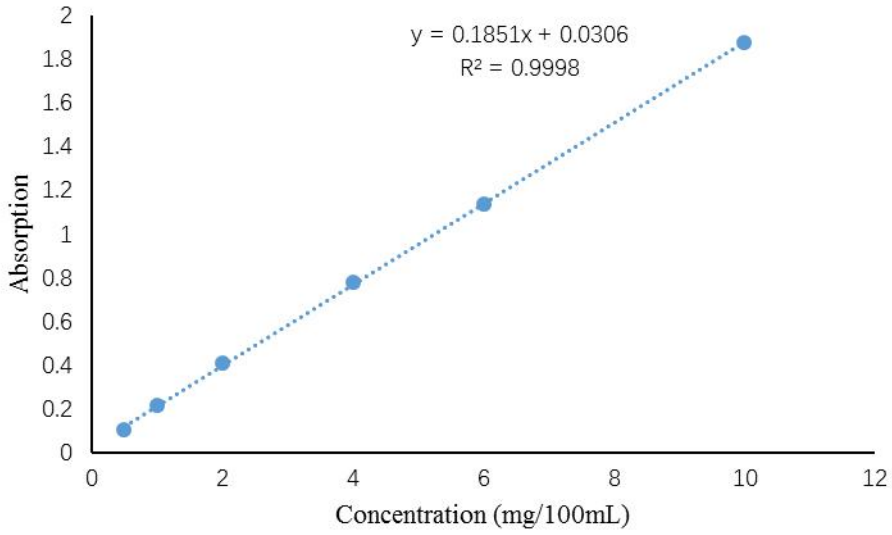

Figure 4.1 UV-Vis absorption against the concentration of **3a** in methanol.

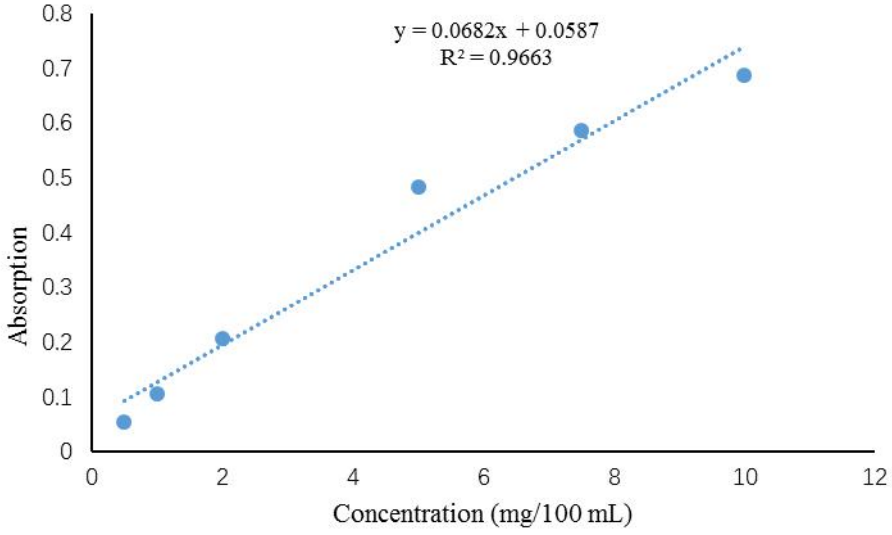

Figure 4.2 UV-Vis absorption against the concentration of **3b** in methanol.

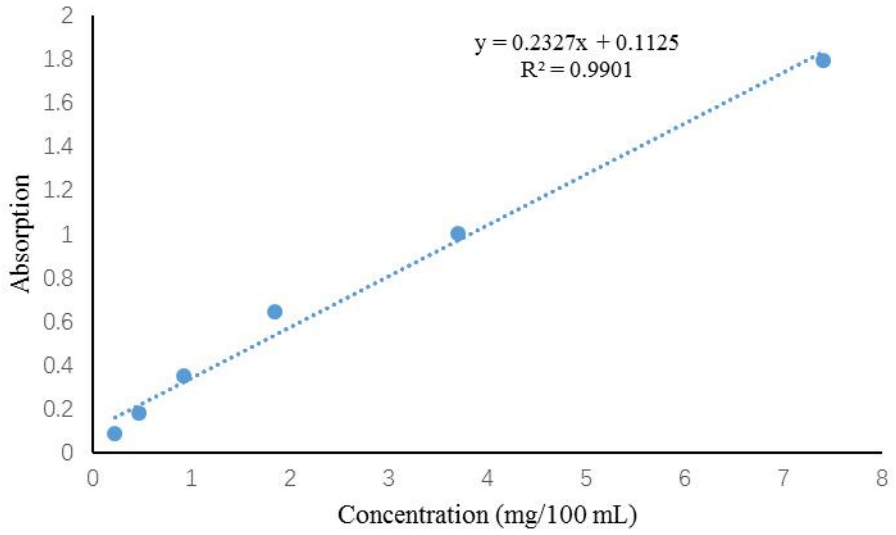

Figure 4.3 UV-Vis absorption against the concentration of **3c** in methanol.

Compound **3a** (60 mg) was dissolved in DCM (6 mL), the mixture was divided between three 7 ml vials and the solvent was evaporated. Methanol (5 mL) was added to each of the concentrated samples and the mixture was submerged in a water bath (37 °C) for 24 h, which was deemed to be a sufficient period (82) to allow the solvent to become saturated with **3a**. An aliquot (1 mL) of the sample was pipetted from the vial, diluted with methanol to a volume of x mL (refer to Table 4.2 for dilution factors) and the absorption measured using a UV-Vis spectrometer.

The solubility of **3b** and **3c** were measured *via* the same procedure as that for **3a**. The data, including the three original absorption measurements, average absorption, the standard curve equation, dilution factor and also the calculated concentrations are listed in Table 4.2.

The solubility measurement of **3a-c** in the mixture of solvent methanol and water (2:1, 1:1) was also attempted, but the UV-Vis results showed no significant signal for these samples, indicating their lack of solubility in this solvent mixture. Three replicates for each compound in same conditions were processed simultaneously and averaged in order to determine the practical operation error.

Table 4.2 Data of solubility measurement for **3a-c** in methanol.

	3a	**3b**	**3c**
Absorption 1	1.235	0.550	0.613
Absorption 2	1.242	0.553	0.618
Absorption 3	1.237	0.552	0.617
Average absorption	1.238	0.538	0.616
Absorption equation	y = 0.0682x + 0.0587	y = 0.0682x + 0.0587	y = 0.2327x + 0.1125
Diluted concentration	6.52 mg/100 mL	7 mg/100 mL	2.16 mg/100 mL
Dilution factor	25	10	25
Concentration (solubility)	**163 mg/100 mL**	**70 mg/100 mL**	**54 mg/100 mL**

4.2 Solubility measurement of 6a and 6c

Five sequential concentrations of each of compounds **6a** and **6c** were prepared in methanol and the corresponding UV-Vis absorption at 665 nm were obtained using the same equipment as that used for UV-Vis spectrum (Table 4.3). The standard curves for each component were plotted (Figures 4.4 and 4.5, respectively) and the equations for linear line of best fit and R^2 were calculated.

Table 4.3 UV-Vis absorption of **6a, 6c** in sequential concentration under 660 nm.

.

Compound	Concentration in methanol (mg/ 100 mL)	Absorption
6a	6.09	2.271
	3.045	1.202
	1.5225	0.589
	0.75516	0.282
	0.38976	0.161
6c	3.38	0.973
	1.69	0.468
	0.845	0.191
	0.4225	0.124
	0.20956	0.066

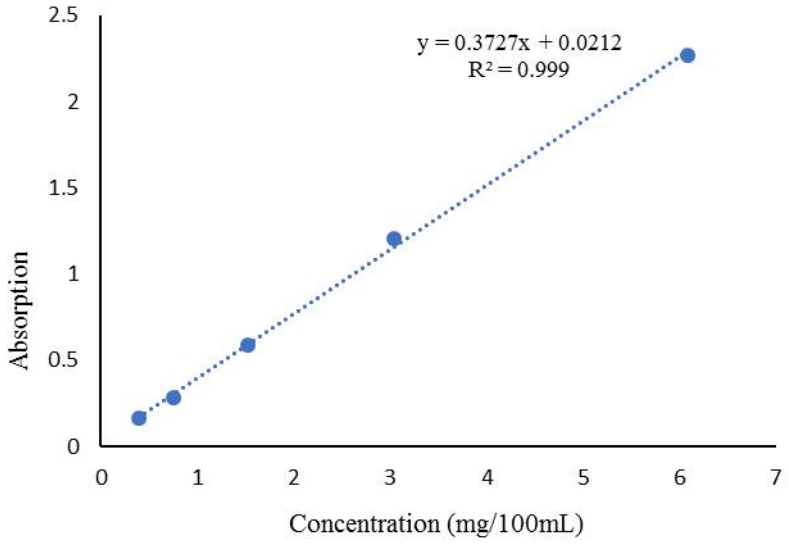

Figure 4.4 UV-Vis absorption against the concentration of **6a** in methanol.

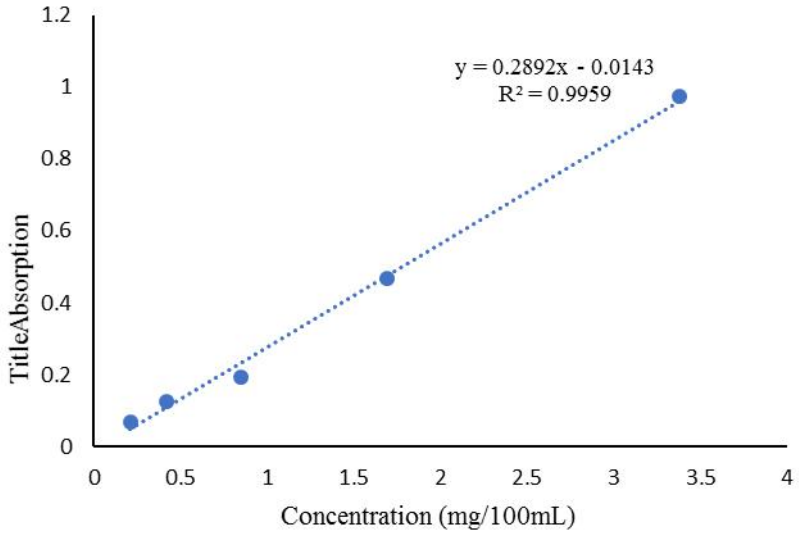

Figure 4.5 UV-Vis absorption against the concentration of **6c** in methanol.

Compound **6a** (10 mg) was dissolved in DCM (1 mL) and the mixture was divided into three 1 ml vials before the solvent was evaporated from each vial. Methanol (0.7 mL) was added into the concentrated samples separately, then the mixture was immersed in a water bath (37℃) for 24 hours which was deemed to be an appropriate period to allow the solvent to become saturated with **6a**. An aliquot (0.2 mL) of the sample was pipetted from the tested vial, diluted with methanol (refer to Table 4.4 for dilution factors) and the absorption measured at 660 nm using the UV-Vis spectrophotometer.

The solubility of **6c** in methanol and in the mixture of methanol and water (1:1) was also obtained *via* the same procedure as that for **6a**. The data, including the three measured absorption values, average absorption, the standard curve equation, dilution factor and the calculated concentrations are listed in Table 4.4.

The solubility measurement of **6a** in the mixture of methanol and water (1:1, 2:1), **6c** in the mixture of methanol and water (1:2) was also attempted, but the UV-Vis results showed there were no significant signal for these samples.

Table 4.4 Data of solubility measurement for **6a, 6c**.

	6a in methanol	**6c** in methanol	**6c** in methanol and water 1:1*
Absorption 1	1.187	0.754	0.918
Absorption 2	1.183	0.77	0.831
Absorption 3	1.416	0.869	0.933
Average absorption	1.262	0.798	0.894
Absorption equation	y = 0.3727x + 0.0212	y = 0.2892x - 0.0143	y = 0.2892x - 0.0143
Diluted concentration	3.329 mg/100 mL	2.809 mg/100 mL	3.141 mg/100 mL
Dilution factor	50	40	11.11
Concentration (solubility)	**166.45 mg/100 mL**	**112.36 mg/100 mL**	**34.90 mg/100 mL**

* The sample pipetted from the 1mL test vial had been concentrated under vacuum before dilution for UV-Vis measurement.

4.3 Solubility and polarity

As stated in Section 1.4, the hydrophilicity of drugs to some degree determines their locations in cells and hence could play a crucial role in their abilities as photosensitizing agents both through altering efficiency of light uptake and in their action on the tumor. The solubility and polarity data for compounds **3a-c, 6a** and **6c** are collected and compared (Table 4.5).

Table 4.5 Data of the solubility and polarity for **3a-c, 6a** and **6c**.

	Methanol (mg/100 mL)	Methanol and water (1:1) (mg/100 mL)	R_f*	Retention time
3a	163	_	0.91	15.9 min
3b	70	_	0.91	16.0 min
3c	54	_	0.82	10.2 min
6a	166.45	_	0.1	8.2 min
6c	112.36	34.90	0.05	5.6 min

* Retention factor (R_f): obtained from the development of silica gel 60 F_{254} coated thin-layer chromatography (TLC) with DCM: Methanol 20:1 as the developing solvent.

Comparison of the solubility data reveals a decreasing trend from **3a** to **3c** in methanol with the value for **3a** being more than twice that of **3b** and triple that of **3c**. In addition, there was no detectable solubility for these three compounds when increasing the polarity of the solvent (methanol: water 1:1, 2:1). The less polar compounds, **3a-c,** interact with polar solvent methanol *via* hydrogen bonds (N-H on the pyrrole ring and O-H on methanol) and the London dispersion forces, leading to their dissolution in methanol. Although the hydrogen bond is much stronger than London dispersion forces generally, in this case, the latter dominates as the only two N-H groups are tightly surrounded by the large flat chlorin ring.

These results indicated that **3a** interacts most with methanol molecules while **3c** has the least interaction, which could be explained by their distinctive space structure on C-17[3] since the other part of **3a**, **3b** and **3c** is same. Compound **3a,** with a long aliphatic chain, has a flexible spatial structure, thus possessing more interacting site with the surrounding molecules *via* London dispersion forces. The attached hexatomic and pentatomic rings in the cholesterol residue of **3b** restricts its spatial flexibility, whereas the molecular residue also has considerable London dispersion force thanks to its large molecular mass and bulky size. According to the same logic, the benzyl ring plane of **3c**, which is more rigid than the other two side chains, contributes to its lowest solubility in methanol.

This rule could be applied once more when explaining the solubility difference between **6a** and **6c** (166.45 to 112.36 mg/ 100 mL). Because of the triglycine ester, a polar group, introduced on C-3[1] position, **6a** and **6c** show increased solubility by comparison with **3a** and **3c**, respectively, due to the additional hydrogen bonding force. Similarly, the polarity for both is increased relative to the precursor compound with retention times changing from 15.9 min to 8.2 min, 10.2 min to 5.6 min and R_f value from 0.91 to 0.1, 0.82 to 0.05, respectively.

The increase in solubility from **3a** to **6a** (+ 4.45 mg/ mL) is more than 10 times less than that from **3c** to **6c** (+ 58 mg/ mL), which suggests that for **3a** and **6a**, the key reason for the high solubility is attributable to the long hydrocarbon chain on C-17[3], while for **3c** and **6c**, the greater rise in solubility should be attributed to the triglycine group on C-3[1].

When introducing the highly polar solvent water into the solvent system, London dispersion forces, the main interacting force between water and the least polar compounds **3a**, **3b**, **3c** was much weaker than the dipole-dipole force and hydrogen bond among water/ methanol molecules, therefore they could barely dissolve in the water-containing system.

The most polar compound, **6c,** shows a low solubility in the polar mixture solvent (methanol: water 1:1), while **6a** fails to dissolve. However, this advantage in **6c** does not continue after increasing the ratio of water to twice volume of methanol.

These results reveal that the introduction of triglycine residue increases the hydrophilicity to some degree and more specific tests *in vivo* will be required for the potential or precursor of PDT candidates.

5. Summary and conclusion

The research objectives listed in Section 1.5 were mostly achieved with failure to obtain triglycine derivative of pyropheophorbide *a* cholesterol ester, the reason for which was elaborated in Section 3.4.

Five derivatives of pyropheophorbide *a* were obtained with four of them believed to be novel compounds (**3a, 3c, 6a,** and **6c**). ^{1}H-NMR and MS data confirmed their structures, while the UV-vis spectra showed **3a-c** have identical maximum absorption wavelength (665 nm in red range), the same as that between **6a** and **6c** (660 nm in red range). The MS^n dissociation diagram provides corresponding fragmentation information and reveal that, although **3a-c** possess similar structures, the neutral losses did show obvious distinguishing patterns. For example, the loss of the entire 2-methoxyl phenol group was observed in MS^2 of **3c**, leaving a carbonyl residue on C-17[3] where there were acid group left for MS^2 of **3a** and **3b**.

RP-HPLC and TLC offered consistent indications of polarity tendency for these five derivatives: (1) triglycine derivatives (**6a** and **6c**) exhibit more polar character than **3a-c**; (2) **3c** and **6c** are more polar than **3a** and **6a**, respectively; (3) **3b** demonstrated identical polarity behavior with **3a**. The more polar compounds **6a** and **6c** dissolved more in polar solvent methanol than **3a-c**, and when increasing the solvent polarity (introducing 50% water), only **6c** showed weak solubility.

The work included in this thesis illustrates a typical process in progressing research and enriched the study of PDT.

6. Experimental

Pyropheophytin *a* (**1**, Scheme 1, Chapter 2) was converted to pyropheophorbide *a* (**2**, Scheme 1, Chapter 2) in the presence of conc. HCl. The free acid product was esterified at the C-17[3] position (shown in **1**) on the macrocycle, obtaining three different types of pyropheophorbide *a* ester (**3a-c,** Scheme 1, Chapter 2).

The triglycine derivatives of **3a, 3c** (**6a, 6c,** Scheme 2, Chapter 3) were obtained through hydroxylation of the C-3 vinyl group, followed by esterification between the 3-(1-hydroxyethyl) group and tert-butyloxycarbonyl (Boc) protected triglycine, followed by Boc deprotection. The attempted preparation of the triglycine derivative of **3b** (compound **12,** Schemes 3 and 4, Chapter 3**)** failed to produce the desired product by three different approaches (Schemes 2-4, Chapter 3) that were attempted.

The structures of all synthesized compounds were confirmed through analysis of the spectra obtained by ESI-MS and ^{1}H-NMR. In addition, the derivatives (**3a-c, 6a, 6c**) of pyropheophorbide *a* were analyzed by UV-vis, RP-HPLC and ESI-MS^{n}.

Purification by silica gel column chromatography was performed as follows: columns were slurry packed with silica gel 60 Å (Sigma Aldrich) saturated with the initial eluent (prepared by stirring with a glass rod until it became a free-flowing slurry with no bubbles present. After loading, most of the eluent above the silica layer was drained out by applying gentle pressure of nitrogen, leaving a thin layer of eluent just above the surface. The “dry loading” method was used to prepare the sample for separation. A mixture of a specific amount of silica gel sample dissolved in an appropriate solvent was gently evaporated under vacuum to give a dry, homogeneous and free-flowing powder. The prepared mixture of silica saturated with sample was loaded evenly and level across the top of the packed column and was capped by two centimeters of low-iron sand. Four column sizes were used: column A (diameter: 3.18 cm), column B (diameter: 2.23 cm), column C (diameter: 1.91 cm) and a glass Pasteur pipette.

6.1 Preparation of pyropheophorbide *a* esters

6.1.1 Pyropheophorbide *a* (2)

Pyropheophorbide *a* was prepared following the procedure of Li *et al.* (65) Briefly, chlorophyll tar (12.0 g), mainly containing pyropheophytin *a*, was dissolved in diethyl ether (100 mL), to which concentrated hydrochloric acid (250 mL) was added over an ice-water bath. The solution was magnetically stirred for 16 h. Diethyl ether in the reaction mixture was evaporated under vacuum and the remaining aqueous phase was washed with *n*-hexane until the organic phase was colourless. The acid phase was diluted with deionised water (2 L), extracted with DCM (200 mL × 3). The combined DCM phase was washed with deionised water (150 mL × 3) and dried over anhydrous sodium sulfate. Removal of the solvent gave crude pyropheophorbide *a* (715 mg) as a black solid, which was purified by silica gel column chromatography to give the target compound (**2**, 350 mg, black solid).

The detailed chromatography method was as follows. Column A was packed with 50 g silica gel, and the sample was adsorbed onto 1.43 g silica gel. The less polar impurities were eluted using an eluent mixture of DCM, methanol and acetic acid (100:5:1, 210 mL). The target compound was eluted by increasing the methanol content to 10 (100:10:1, 660 mL).

6.1.2 Pyropheophorbide *a* 1-octadecanol ester (3a)

A flask (100 mL) was charged with pyropheophorbide *a* (**2**, 150 mg, 0.28 mmol), 1-octadecanol (151.5 mg, 0.56 mmol), EDC (80.5 mg, 0.42 mmol), HOBt (56.8 mg, 0.42 mmol), DMAP (34.2 mg, 0.28 mmol) and Et_3N (0.117 mL, 0.84 mmol) in DCM (30 mL). After magnetically stirring at room temperature for 24 h, the reaction mixture was washed with diluted hydrochloric acid (3%, 15 mL × 2), deionized water (15 mL × 3) and dried over anhydrous sodium sulfate. Removal of the solvent gave crude product that was purified by silica gel column chromatography to give the target compound (**3a**, 100 mg, black solid, yield: 45.3%).

The detailed chromatography method was as follows. Column B was packed with silica gel (18.6 g), and the sample adsorbed onto silica gel (0.62 g). The less polar impurities were eluted with a mixture of *n*-hexane and ethyl acetate (10:1, 275 mL; 7:1, 300 mL). The target compound was eluted by increasing the proportion of ethyl acetate (5:1, 480 mL).

6.1.3 Pyropheophorbide *a* cholesterol ester (3b)

The preparation procedure for **3b** (130 mg, black solid, yield: 51.3%) was the same as for **3a** but with cholesterol (216.5 mg, 0.56 mmol) in place of 1-octadecanol.

The detailed chromatography method was as follows. Column B was packed with silica gel (21 g), and the sample was adsorbed onto silica gel (0.7 g). The less polar impurities were eluted with a mixture of *n*-hexane and acetone (10:1, 220 mL; 7:1, 114 mL). The target compound was eluted by increasing the ratio of acetone (5:1, 240 mL).

6.1.4 Pyropheophorbide *a* 2-methoxyl phenol ester (3c)

The preparation procedure for **3c** (100 mg, black solid, yield: 55.6%) was the same as for **3a** but with 2-methoxyl phenol (61.6 μL, 0.56 mmol) in place of 1-octadecanol.

The detailed chromatography method was as follows. Column B was packed with 18 g silica gel, and the sample was adsorbed onto 0.6 g silica gel. The less polar impurities were eluted with a mixture of *n*-hexane and ethyl acetate (10:1, 220 mL; 5:1, 240 mL). The target compound was eluted by increasing the ratio of ethyl acetate (3:1, 400 mL).

6.2 Preparation of the derivatives of pyropheophorbide *a* esters

6.2.1 3-(1-hydroxyethyl) pyropheophorbide *a* octadecanol ester (4a)

The mixture of **3a** (158 mg, 0.20 mmol) and hydrobromic acid solution (33% wt. in acetic acid, 5 mL) was stirring at 0°C for 2 h and at room temperature for 14 h. The solvent was removed under nitrogen and 5 mL acetone and 1 mL water were added into the residue at 0°C. After one-hour stirring, the reaction was neutralized with 4%

sodium hydrocarbonate aqueous solution, followed by extraction with blended mixture of DCM and methanol (3:1, 15 mL × 4). The combined organic phase was washed with deionized water (20 mL × 2) and dried over anhydrous sodium sulfate. Purification by silica gel column chromatography gave the target compound (**4a**, 55 mg, black solid, yield: 34.0%).

The detailed chromatography method was as follows. Column B was packed with 19 g silica gel, and the sample was adsorbed onto 0.38 g silica gel. Impurities were eluted with mixtures of *n*-hexane and ethyl acetate (10:1, 110 mL; 5:1, 120 mL). The target compound was eluted by increasing the proportion of ethyl acetate (10:3, 390 mL).

6.2.2 3-(1-hydroxyethyl) pyropheophorbide *a* cholesterol ester (4c)

The preparation procedure for **4c** (55 mg, black solid, yield: 53.6%) from **3c** (100 mg, 0.16 mmol) was the same as for **4a**.

The detailed chromatography method was as follows. Column B was packed with silica gel (4 g), and the sample was adsorbed onto silica gel (0.2 g). Impurities were eluted with mixtures of *n*-hexane and ethyl acetate (5:1, 120 mL; 3:1, 160 mL). The target compound was eluted by increasing the ratio of ethyl acetate (2:1, 150 mL; 1:1, 200 mL).

6.2.3 Boc-gly-gly-gly-OH ester of 4a (5a)

A flask (50 mL) was charged with **4a** (50 mg, 62.1 μmol), Boc-Gly-Gly-Gly-OH (26.9 mg, 93.2 μmol), EDC (26.8 mg, 0.140 mmol), HOBt (18.8 mg, 0.140 mmol), 4-DMAP (11.4 mg, 93.2 μmol) and Et_3N (39 μL, 0.28 mmol) in DCM (10 mL). After stirring at room temperature for 24 h, the reaction mixture was washed with diluted hydrochloric acid (3%; 10 mL × 2), deionized water (10 mL × 3) and dried over anhydrous sodium sulfate. Removal of the solvent gave crude product that was purified by silica gel column chromatography to give target compound (**5a**, 35 mg, black solid, yield: 52.4%).

The detailed chromatography method was as follows. Column C was packed with silica gel (9 g), and the sample was adsorbed onto silica gel (0.3 g). Impurities were

eluted with mixtures of DCM and methanol (100:1, 50.5 mL; 75:1, 76 mL). The target compound was eluted by increasing the ratio of methanol (50:1, 120 mL).

6.2.4 Boc-gly-gly-gly-OH ester of 4c (5c)

The preparation procedure for **5c** (30 mg, black solid, yield: 39.9%) from **4c** (53.3 mg, 80.96 μmol) was the same as for **5a**.

The detailed chromatography method was as follows. Column C was packed with silica gel (10 g), and the sample was adsorbed onto silica gel (0.33 g). Impurities were eluted with a mixture of DCM and acetone (5:1, 60 mL). The target compound was eluted by increasing the ratio of acetone (2:1, 75 mL).

6.2.5 Gly-gly-gly-OH ester of 5a (6a)

Compound **5a** (15 mg, 13.9 μmol) was dissolved in DCM (1.5 mL) and trifluoroacetic acid (0.3 mL) was added. The reaction was stirred for 2 h at 0°C. After the solvent was removed under nitrogen, the residue was dissolved in DCM (1 mL) and Et_3N was used to neutralize the remaining acid. After evaporation of the solvent the crude product was purified by silica gel chromatography to obtain the target compound (**6a**, 7 mg, black solid, yield: 51.4%).

The detailed chromatography method was as follows. A glass Pasteur pipette was packed with silica gel (0.4 g), and the sample, dissolved in DCM 0.5 mL), was loaded onto the top of the column. Impurities were eluted with DCM (20 mL) and the target compound with a mixture of DCM and methanol (10:1, 5.5 mL).

6.2.6 Gly-gly-gly-OH ester of 5c (6c)

Compound **5c** (20 mg, 21.5 μmol) was dissolved in DCM (2 mL) and trifluoroacetic acid (0.4 mL) was added. The reaction was stirred for 2 h at 0°C. After the solvent was removed under nitrogen, the residue was dissolved in DCM (1.5 mL) and Et_3N was used to neutralize the remaining acid. After evaporation of the solvent the crude product was purified by silica gel chromatography to obtain the target compound (**6c**, 10 mg, black solid, yield: 56.0%)

The detailed chromatography method was as follows. A glass Pasteur pipette was packed with silica gel (0.6 g) and the sample, dissolved in DCM (0.5 mL), was loaded onto the top of the column. Impurities were eluted with DCM (25 mL) and the target compound with a mixture of DCM and methanol (10:1, 11 mL).

6.2.7 Benzyl protection of pyropheophorbide *a* (7)

To the flask (100 mL) charged with crude compound **2** (460 mg, 0.86 mmol) and dimethyl formamide (50 mL), potassium carbonate (178 mg, 1.29 mmol) was added followed by benzyl bromide (153 μL, 1.29 mmol) at 0°C. After 2 h the reaction was diluted with deionized water (100 mL) and extracted with DCM (40 mL × 3). The combined organic phase was washed with deionized water (40 mL × 3) and dried over anhydrous sodium sulfate. Removal of the solvent gave crude product that was purified by silica gel column chromatography to give the target compound (**7**, 188 mg, black solid).

The detailed chromatography method was as follows. Column A was packed with silica gel (40 g), and the sample was adsorbed onto silica gel (2.0 g). The impurities were eluted with mixtures of *n*-hexane and ethyl acetate (10:1, 110 mL; 5:1, 240 mL; 2:1, 150 mL). The target compound was eluted by increasing the ratio of ethyl acetate (2:1, 300 mL).

6.2.8 3-(1-hydroxyethyl) pyropheophorbide *a* benzyl ester (8)

A mixture of **7** (170 mg, 0.27 mmol) and hydrobromic acid solution (33% wt. in acetic acid, 9 mL) was stirring at 0°C for 2 h and at room temperature for 14 h. The solvent was removed under nitrogen and 9 mL acetone and 2 mL water were added to the residue at 0°C. After stirring for 1 h the reaction was neutralized with 4% sodium hydrocarbonate aqueous solution, followed by the extraction with solvent mixture of DCM and methanol (3:1, 20 mL × 4). The combined organic phase was washed with deionized water (20 mL × 2) and dried over anhydrous sodium sulfate. The crude product (242 mg) was obtained by evaporating the solvent under vacuum.

To the flask (50 mL) charged with the crude product (242 mg) and dimethyl formamide (25 mL), potassium carbonate (91 mg, 0.66 mmol) followed by benzyl

bromide (57.2 μL, 0.48 mmol) were added at 0°C. After 2 h the reaction was diluted with deionized water (25 mL) and extracted with DCM (25 mL × 3). The combined organic phase was washed with deionized water (30 mL × 3) and dried over anhydrous sodium sulfate. Removal of the solvent gave crude product which was purified by silica gel column chromatography to give the target compound (**8**, 101 mg, black solid, yield: 58.2%).

The detailed chromatography method was as follows. Column A was packed with silica gel (27 g), and the sample was adsorbed onto silica gel (0.94 g). Impurities were eluted with a mixture of *n*-hexane and ethyl acetate (5:1, 120 mL). The target compound was eluted by increasing the ratio of ethyl acetate (4:1, 125 mL).

6.2.8 Boc-gly-gly-gly-OH ester of 8 (9)

A flask (25 mL) was charged with **8** (74 mg, 0.115 mmol), Boc-gly-gly-gly-OH (50 mg, 0.173 mmol), EDC (66.3 mg, 0.346 mmol), 1-HOBt (46.8 mg, 0.346 mmol), 4-DMAP (21.1 mg, 0.173 mmol) and Et_3N (72 μL, 0.518 mmol) in DCM (10 mL). After stirring at room temperature for 24 h, the reaction mixture was washed with dilute hydrochloric acid (3%; 10 mL × 2), deionized water (10 mL × 3) and dried over anhydrous sodium sulfate. Removal of the solvent gave crude product that was purified by silica gel column chromatography to give the target compound (**9**, 30 mg, black solid, yield: 30.6%).

The detailed chromatography method was as follows. Column A was packed with silica gel (25 g), and the sample was adsorbed onto silica gel (0.99 g). Impurities were eluted with mixtures of DCM and methanol (100:1, 303 mL; 50:1, 102 mL). The target compound was eluted by increasing the ratio of methanol (25:1, 208 mL).

6.2.9 3-(1-hydroxyethyl) pyropheophorbide *a* (13)

A mixture of **2** (150 mg, 0.28 mmol) and hydrobromic acid solution (33%wt. in acetic acid, 15 mL) was stirring at 0°C for 2 h and at room temperature for 14 h. The solvent was removed under nitrogen and 10 mL acetone and 2 mL water were added into the residue at 0°C. After stirring for 1 h the reaction was neutralized with 4% sodium hydrocarbonate aqueous solution, followed by extraction with a mixture of

DCM and methanol (3:1, 15mL × 4). The combined organic phase was washed with deionized water (20 mL × 2) and dried over anhydrous sodium sulfate. Purification by silica gel column chromatography gave target compound (**13**, 60 mg, black solid, yield: 38.7%).

The detailed chromatography method was as follows. Column B was packed with silica gel (20 g), and the sample was adsorbed onto silica gel (0.40 g). Impurities were eluted with mixtures of DCM and methanol (100:1, 202 mL; 50:1, 204 mL). The target compound was eluted by increasing the ratio of methanol (20:1, 210 mL).

6.2.10 Acetyl protected compound 13 (14)

Compound **13** (46.5 mg, 0.084 mmol) was dissolved in 10 mL pyridine, to which acetyl chloride (24 μL, 0.33 mmol) was added dropwise at 0°C. After stirring for 2 h at 0°C, the solvent was evaporated under vacuum before the residue was dissolved in 10 mL DCM. The mixture was washed with 2% hydrochloric acid solution (10 mL × 3), deionized water (10 mL × 2) and dried over anhydrous sodium sulfate. Purification by silica gel column chromatography gave target compound (**14**, 27 mg, black solid, yield: 53.9%).

The detailed chromatography method was as follows. Column C was packed with silica gel (2 g), and the sample was adsorbed onto silica gel (0.1 g). Impurities were eluted with mixtures of DCM and methanol (100:1, 50.5 mL; 50:1, 51 mL). The target compound was eluted by increasing the ratio of methanol (20:1, 105 mL).

6.3 Analysis

6.3.1 ^{1}H-NMR

^{1}H-NMR spectra of all of the synthesized products were obtained using a JEOL ECS 400 MHz spectrometer with 8 or 16 scans. A single pulse with 5 μs pulse width and 5 s pulse delay were applied in detection. The number of sampling data points was 16384 (32768 after zero filling) and the spectra were obtained after Fourier transformation. Samples were prepared in deuterated chloroform ($CDCl_3$).

6.3.2 MS and MS^n

MS were generated on a Brucker HCT ultra ETD II ion trap spectrometer using ESI (operated in positive ion mode). The injection flow rate was 180 µL/h, with the nebulizer set to 10 psi, dry gas flow rate of 5 L/min and a drying temperature of 300°C. Multistage mass spectra were obtained up to MS^4/MS^5 using a fragmentation amplitude of 1.5 V (SmartFrag 30-200%) with isolation width set as 3 *m/z*.

6.3.3 UV-vis

Spectras were obtained using an Agilent Varian Cary® 50 spectrophotometer. The scan speed and slit width were set to fast and 0.1 nm, respectively, with the range between 330 and 800 nm. All samples were prepared in methanol and analyzed in a cuvette with 1 cm pathlength.

6.3.4 RP-HPLC-UV-vis and TLC

RP-HPLC was performed using a Thermo Dionex UltiMate® 3000 Rapid Separation LC system comprising a quaternary pump (LPG-3400RS), an autosampler and a diode array detector (DAD-3000RS), controlled by Chromeleon 6.8 software. Separation was achieved using a two Waters Spherisorb ODS2 cartridge columns (150 mm x 4.6 mm i.d.; 3 µm) coupled in series. A mixture of ethyl acetate and methanol (1:1) was used as the mobile phase with flow rate and analysis time set to 1 mL/min and 30 min, respectively. Samples were prepared in acetone for injection (5 µL).

TLC was used during all the synthesis procedures when necessary and TLC plates were coated with silica gel 60 F254 with appropriate developing solvent.

6.3.5 Solubility measurement

The solubility of pyropheophorbide *a* derivatives **3a-c** and **6a, 6c** at 37 ℃ were

measured using a temperature-controlled water bath (Thermo Haake DC10 with bath B3) and UV-Vis spectrometer (Agilent Varian Cary® 50). The detail of measurement practice has been elaborated in Section 2.3.3 for **3a-c** and Section 3.5.3 for **6a, 6c**, respectively.

Abbreviation

AK: actinic keratosis

ALA: aminolevulinic acid

Boc-Gly-Gly-Gly-OH: *N*-(tert-butoxycarbonyl) triglycine

BPD-MA: benzoporphyrin derivative monoacid ring

DADP-a: 5, 10-di[4-*N*-trimethylaminophenyl]-15, 20-diphenylporphyrin

DADP-o: 5, 15-di[4-(*N*-trimethylaminophenyl)-10, 20-diphenylporphyrin

DCC: dicyclohexylcarbodiimide

DCM: dichloromethane

DHE: dihematoporphyrin ether

DMAP: *N, N*-dimethylpyridin-4-amine

DP: deuteroporphyrin IX

DPPC: dipalmitoyl phosphatidylcholine

EDC: *N*-(3-dimethylaminopropyl)-*N*'-ethylcarbodiimide hydrochloride

ESI-MS: electrospray ionization mass spectrometry

ESI-MS^n: electrospray ionization multistage mass spectrometry

Et_3N: triethyl amine

HAL: hexaminolevulinate

^{1}H-NMR: proton nuclear magnetic resonance spectroscopy

HOBt: 1-hydroxybenzotriazole hydrate

HP: hematoporphyrin

Hp: hematoporphyrin

HpD: hematoporphyrin derivative

HPPH: 2-(1-hexyloxyethyl)-2-devinyl pyropheophorbide *a*

LDL: low density lipoprotein

MAbs: monoclonal antibodies

MAL: methyl ester of aminolevulinic acid

NHS: *N*-hydroxysuccinimide

NPe6: *N*-aspartyl chlorin e6

Pc 4: phthalocyanine 4

Pd-C: palladium on carbon

PDT: photodynamic therapy

Pheo: pheophorbide *a*

PPIX: protoporphyrin IX

PS: photosensitizer

PSs: photosensitizers

R_f: retention factor

ROS: reactive oxygen species

RP-HPLC: reversed phase-high performance liquid chromatography

SnET2: tin ethyl etiopurpurin

TFA: trifluoroacetic acid

m-THPC: meta-tetra-(hydroxyphenyl) chlorin

TLC: thin-layer chromatography

UV-vis: ultraviolet-visible

References

1. Hu, Y., Huang, X., Lu, S., Hamblin, M.R., Mylonakis, E., Zhang, J. and Xi, L. (2015) Photodynamic therapy combined with terbinafine against chromoblastomycosis and the effect of PDT on Fonsecaea monophora in vitro. *Mycopathologia*, **179**, 103-109.
2. Juarranz, Á., Jaén, P., Sanz-Rodríguez, F., Cuevas, J. and González, S. (2008) Photodynamic therapy of cancer. Basic principles and applications. *Clinical and Translational Oncology*, **10**, 148-154.
3. Holder, A. and LLagostera, D. (2008) Optimal treatments for photodynamic therapy. *4OR*, **6**, 167-182.
4. Nowis, D., Makowski, M., Stokłosa, T., Legat, M., Issat, T. and Gołąb, J. (2005) Direct tumor damage mechanisms of photodynamic therapy. *Acta Biochimica Polonica*, **52**, 339-352.
5. Helander, L. (2015) Hexylaminolevulinate photodynamic treatment of cancer cell lines. Norwegian University of Science and Technology.
6. Yavari, N. (2006) Optical spectroscopy for tissue diagnostics and treatment control. University of Bergen.
7. Moan, J. and Peng, Q. (2003) In Patrice, T. (ed.), *Photodynamic Therapy*. The Royal Society of Chemistry, Vol. 2, pp. 1-18.
8. Hausmann, W. (1910) *Über die sensibilisierende Wirkung des Hämatoporphyrins*.
9. Cripps, D. (1985) Porphyria: genetic and acquired. *IARC Scientific Publications*, 549-566.
10. Auler, H. and Banzer, G. (1942) Untersuchungen über die Rolle der Porphyrine bei geschwulstkranken Menschen und Tieren. *Journal of Cancer Research and Clinical Oncology*, **53**, 65-68.
11. Dougherty, T.J., Lawrence, G., Kaufman, J.H., Boyle, D., Weishaupt, K.R. and Goldfarb, A. (1979) Photoradiation in the treatment of recurrent breast carcinoma. *Journal of the National Cancer Institute*, **62**, 231-237.
12. Dougherty, T., Boyle, D., Weishaupt, K., Henderson, B., Potter, W., Bellnier, D. and Wityk, K. (1983), *Porphyrin Photosensitization*. Springer, pp. 3-13.
13. Huang, Z. (2005) A review of progress in clinical photodynamic therapy. *Technology in Cancer Research & Treatment*, **4**, 283-293.
14. Porfimer sodium. 2015,Jul. Available from: https://en.wikipedia.org/wiki/Porfimer_sodium.
15. Freitag, L., Ernst, A., Thomas, M., Prenzel, R., Wahlers, B. and Macha, H. (2004) Sequential photodynamic therapy (PDT) and high dose brachytherapy for endobronchial tumour control in patients with limited bronchogenic carcinoma. *Thorax*, **59**, 790-793.
16. Bae, S.M., Huh, S.W., Park, E.K., Lee, K.H., Lee, J.M., Namkoong, S.E., Han, S.J., Kim, C.K., Kim, J.K. and Kim, Y.W. (2003) Photogem induces necrosis in various uterine cervical cancer cell lines by PDT. *Cancer Res Treat*, **35**, 549-556.
17. Wan, M.T. and Lin, J.Y. (2014) Current evidence and applications of photodynamic therapy in dermatology. *Clinical, Cosmetic and Investigational Dermatology*, **7 (1)**, 145-163.
18. Hongcharu, W., Taylor, C.R., Aghassi, D., Suthamjariya, K., Anderson, R.R. and Chang, Y. (2000) Topical ALA-photodynamic therapy for the treatment of acne vulgaris. *Journal of Investigative Dermatology*, **115**, 183-192.
19. Pinto, C., Schafer, F., Orellana, J.J., Gonzalez, S. and Hasson, A. (2013) Efficacy of red light alone and methyl-aminolaevulinate-photodynamic therapy for the treatment of mild and moderate facial acne. *Indian Journal of Dermatology, Venereology, and Leprology*, **79**, 77.
20. Gardlo, K., Horska, Z., Enk, C.D., Rauch, L., Megahed, M., Ruzicka, T. and Fritsch, C. (2003) Treatment of cutaneous leishmaniasis by photodynamic therapy. *Journal of the American Academy of Dermatology*, **48**, 893-896.
21. Sohl, S., Kauer, F., Paasch, U. and Simon, J.C. (2007) Photodynamic treatment of cutaneous leishmaniasis. *JDDG: Journal der Deutschen Dermatologischen Gesellschaft*, **5**, 128-130.
22. Ericson, M.B., Wennberg, A. and Larko, O. (2008) Review of photodynamic therapy in actinic keratosis and basal cell carcinoma. *Therapeutics and Clinical Risk Management*, **4**, 1.
23. Furre, I.E., Shahzidi, S., Luksiene, Z., Møller, M.T., Borgen, E., Morgan, J., Tkacz-Stachowska, K., Nesland, J.M. and Peng, Q. (2005) Targeting PBR by hexaminolevulinate-mediated photodynamic therapy induces apoptosis through translocation of apoptosis-inducing factor in human leukemia cells. *Cancer Research*, **65**, 11051-11060.
24. Fingar, V., Kik, P., Haydon, P., Cerrito, P., Tseng, M., Abang, E. and Wieman, T. (1999) Analysis of acute vascular damage after photodynamic therapy using benzoporphyrin derivative (BPD). *British Journal of Cancer*, **79**, 1702.

25. Rousset, N., Bourre, L. and Thibaud, S. (2003). Royal Society of Chemistry: Cambridge, UK, pp. 59-80.
26. Triesscheijn, M., Ruevekamp, M., Aalders, M., Baas, P. and Stewart, F.A. (2005) Outcome of mTHPC mediated photodynamic therapy is primarily determined by the vascular response. *Photochemistry and Photobiology*, **81**, 1161-1167.
27. Dolmans, D.E., Fukumura, D. and Jain, R.K. (2003) Photodynamic Therapy for Cancer. *Nature Reviews Cancer*, **3**, 380-387.
28. O'Connor, A.E., Gallagher, W.M. and Byrne, A.T. (2009) Porphyrin and nonporphyrin photosensitizers in oncology: preclinical and clinical advances in photodynamic therapy. *Photochemistry and Photobiology*, **85**, 1053-1074.
29. Usuda, J., Kato, H., Okunaka, T., Furukawa, K., Tsutsui, H., Yamada, K., Suga, Y., Honda, H., Nagatsuka, Y. and Ohira, T. (2006) Photodynamic therapy (PDT) for lung cancers. *Journal of Thoracic Oncology*, **1**, 489-493.
30. Kobayashi, W., Liu, Q., Nakagawa, H., Sakaki, H., Teh, B., Matsumiya, T., Yoshida, H., Imaizumi, T., Satoh, K. and Kimura, H. (2006) Photodynamic therapy with mono-L-aspartyl chlorin e6 can cause necrosis of squamous cell carcinoma of tongue: Experimental study on an animal model of nude mouse. *Oral Oncology*, **42**, 45-49.
31. Lobel, J., MacDonald, I.J., Ciesielski, M.J., Barone, T., Potter, W.R., Pollina, J., Plunkett, R.J., Fenstermaker, R.A. and Dougherty, T.J. (2001) 2 ‐ [1 ‐ hexyloxyethyl] ‐ 2 ‐ devinyl pyropheophorbide ‐ a (HPPH) in a nude rat glioma model: Implications for photodynamic therapy. *Lasers in Surgery and Medicine*, **29**, 397-405.
32. Ormond, A.B. and Freeman, H.S. (2013) Dye sensitizers for photodynamic therapy. *Materials*, **6**, 817-840.
33. Simmer, K.A. (2014), University of Michigan.
34. Kerdous, R., Sureau, F., Bour, A. and Bonneau, S. (2015) Release kinetics of an amphiphilic photosensitizer by block-polymer nanoparticles. *International Journal of Pharmaceutics*, **495**, 750-760.
35. Brandis, A.S., Salomon, Y. and Scherz, A. (2006), *Chlorophylls and Bacteriochlorophylls*. Springer, pp. 461-483.
36. Moan, J. (1990) Properties for optimal PDT sensitizers. *Journal of Photochemistry and Photobiology B: Biology*, **5**, 521-524.
37. Macdonald, I.J. and Dougherty, T.J. (2001) Basic principles of photodynamic therapy. *Journal of Porphyrins and Phthalocyanines*, **5**, 105-129.
38. Institute, R.P.C., United States, New York, Vol. 2011.
39. Grossweiner LI. Singlet Oxygen: Generation and Properties [Internet]. Available from: http://www.photobiology.com/educational/len2/singox.html.
40. Evans, H.H., Horng, M.F., Ricanati, M., Deahl, J.T. and Oleinick, N.L. (1997) Mutagenicity of photodynamic therapy as compared to UVC and ionizing radiation in human and murine lymphoblast cell lines. *Photochemistry and Photobiology*, **66**, 690-696.
41. Quartarolo, A.D., Russo, N., Sicilia, E. and Adamo, C. (2011), *Photosensitizers in Medicine, Environment, and Security*. Springer, pp. 121-134.
42. Chen, J. (2002). Google Patents.
43. Hopper, C. (2000) Photodynamic therapy: a clinical reality in the treatment of cancer. *The Lancet Oncology*, **1**, 212-219.
44. Köhler, G. and Milstein, C. (1975) Continuous cultures of fused cells secreting antibody of predefined specificity. *Nature*, **256**, 495-497.
45. Del Governatore, M., Hamblin, M.R., Shea, C.R., Rizvi, I., Molpus, K.G., Tanabe, K.K. and Hasan, T. (2000) Experimental photoimmunotherapy of hepatic metastases of colorectal cancer with a 17.1 A chlorine6 immunoconjugate. *Cancer Research*, **60**, 4200-4205.
46. Yemul, S., Berger, C., Estabrook, A., Suarez, S., Edelson, R. and Bayley, H. (1987) Selective killing of T lymphocytes by phototoxic liposomes. *Proceedings of the National Academy of Sciences*, **84**, 246-250.
47. Gueddari, N., Favre, G., Hachem, H., Marek, E., Le Gaillard, F. and Soula, G. (1993) Evidence for up-regulated low density lipoprotein receptor in human lung adenocarcinoma cell line A549. *Biochimie*, **75**, 811-819.
48. Maziere, J., Morliere, P. and Santus, R. (1991) New trends in photobiology: The role of the low density lipoprotein receptor pathway in the delivery of lipophilic photosensitizers in the photodynamic therapy of tumours. *Journal of Photochemistry and Photobiology B: Biology*, **8**, 351-360.
49. Dixit, S., Miller, K., Zhu, Y., McKinnon, E., Novak, T., Kenney, M.E. and Broome, A.-M.

(2015) Dual Receptor-Targeted Theranostic Nanoparticles for Localized Delivery and Activation of Photodynamic Therapy Drug in Glioblastomas. *Molecular Pharmaceutics*, **12**, 3250-3260.

50. Wan, H., Zhang, Y., Zhang, W. and Zou, H. (2015) Robust Two-Photon Visualized Nanocarrier with Dual Targeting Ability for Controlled Chemo-Photodynamic Synergistic Treatment of Cancer. *ACS Applied Materials & Interfaces*, **7**, 9608-9618.
51. Zhang, X., Liu, T., Li, Z. and Zhang, X. (2014) Progress of photodynamic therapy applications in the treatment of musculoskeletal sarcoma (Review). *Oncology Letters*, **8**, 1403-1408.
52. Castano, A.P., Demidova, T.N. and Hamblin, M.R. (2004) Mechanisms in photodynamic therapy: part one—photosensitizers, photochemistry and cellular localization. *Photodiagnosis and Photodynamic Therapy*, **1**, 279-293.
53. Rück, A. and Steiner, R. (1998) Basic reaction mechanisms of hydrophilic and lipophilic photosensitisers in photodynamic tumour treatment. *Minimally Invasive Therapy & Allied Technologies*, **7**, 503-509.
54. Sujatha, J. and Mishra, A. (1998) Phase transitions in phospholipid vesicles: Excited state prototropism of 1-naphthol as a novel probe concept. *Langmuir*, **14**, 2256-2262.
55. Woodburn, K., Vardaxis, N., Hill, J., Kaye, A. and Phillips, D. (1991) Subcellular localization of porphyrins using confocal laser scanning microscopy. *Photochemistry and Photobiology*, **54**, 725-732.
56. Kessel, D., Luguya, R. and Vicente, M.G.H. (2003) Localization and photodynamic efficacy of two cationic porphyrins varying in charge distribution. *Photochemistry and Photobiology*, **78**, 431-435.
57. Geze, M., Morliere, P., Maziere, J., Smith, K. and Santus, R. (1993) Lysosomes, a key target of hydrophobic photosensitizers proposed for photochemotherapeutic applications. *Journal of Photochemistry and Photobiology B: Biology*, **20**, 23-35.
58. Nagata, S., Obana, A., Gohto, Y. and Nakajima, S. (2003) Necrotic and apoptotic cell death of human malignant melanoma cells following photodynamic therapy using an amphiphilic photosensitizer, ATX‐S10 (Na). *Lasers in Surgery and Medicine*, **33**, 64-70.
59. Morgan, J. and Oseroff, A.R. (2001) Mitochondria-based photodynamic anti-cancer therapy. *Advanced Drug Delivery Reviews*, **49**, 71-86.
60. Runnels, J., Chen, N., Ortel, B., Kato, D. and Hasan, T. (1999) BPD-MA-mediated photosensitization in vitro and in vivo: cellular adhesion and β1 integrin expression in ovarian cancer cells. *British Journal of Cancer*, **80**, 946.
61. Takeuchi, Y., Kurohane, K., Ichikawa, K., Yonezawa, S., Nango, M. and Oku, N. (2003) Induction of intensive tumor suppression by antiangiogenic photodynamic therapy using polycation‐modified liposomal photosensitizer. *Cancer*, **97**, 2027-2034.
62. Aveline, B.M. and Redmond, R.W. (1999) Can cellular phototoxicity be accurately predicted on the basis of sensitizer photophysics? *Photochemistry and Photobiology*, **69**, 306-316.
63. Trivedi, N.S., Wang, H.W., Nieminen, A.L., Oleinick, N.L. and Izatt, J.A. (2000) Quantitative Analysis of Pc 4 Localization in Mouse Lymphoma (LY‐R) Cells via Double‐label Confocal Fluorescence Microscopy. *Photochemistry and Photobiology*, **71**, 634-639.
64. Pyropheophorbide *a*. Technical Information. https://www.scbt.com/scbt/product/pyropheophorbide-a-24533-72-0.
65. Li, C., Zheng, J. and Fang, Y. (2002) Synthesis of porphyrin derivative from pyropheophytin-a by 17, 18-dehydrogenation. *Academic Journal of Guangdong College of Pharmacy*, **19**, 19-21.
66. Dunetz, J.R., Magano, J. and Weisenburger, G.A. (2016) Large-Scale Applications of Amide Coupling Reagents for the Synthesis of Pharmaceuticals. *Organic Process Research & Development*, **20**, 140-177.
67. Valeur, E. and Bradley, M. (2009) Amide bond formation: beyond the myth of coupling reagents. *Chemical Society Reviews*, **38**, 606-631.
68. Sheehan, J.C., Preston, J. and Cruickshank, P.A. (1965) A rapid synthesis of oligopeptide derivatives without isolation of intermediates. *Journal of the American Chemical Society*, **87**, 2492-2493.
69. Robl, J.A., Sun, C.-Q., Stevenson, J., Ryono, D.E., Simpkins, L.M., Cimarusti, M.P., Dejneka, T., Slusarchyk, W.A., Chao, S. and Stratton, L. (1997) Dual metalloprotease inhibitors: mercaptoacetyl-based fused heterocyclic dipeptide mimetics as inhibitors of angiotensin-converting enzyme and neutral endopeptidase. *Journal of Medicinal Chemistry*, **40**, 1570-1577.
70. Hagiwara, D., Miyake, H., Igari, N., Karino, M., Maeda, Y., Fujii, T. and Matsuo, M. (1994)

Studies on neurokinin antagonists. 4. Synthesis and structure-activity relationships of novel dipeptide substance P antagonists: N2-[(4R)-4-hydroxy-1-[(1-methyl-1H-indol-3-yl) carbonyl]-L-prolyl]-N-methyl-N-(phenylmethyl)-3-(2-naphthyl)-L-alaninamide and its related compounds. *Journal of Medicinal Chemistry*, **37**, 2090-2099.

71. Kopple, K.D. and Nitecki, D.E. (1962) Reactivity of Cyclic Peptides. II. cyclo-L-Tyrosyl-L-histidyl and cyclo-L-Tyrosyltriglycyl-L-histidylglycyl. *Journal of the American Chemical Society*, **84**, 4457-4464.
72. Newman, M. and Boden, H. (1961) Notes-N-Methylpyrrolidone as Solvent for Reaction of Aryl Halides with Cuprous Cyanide. *Journal of Organic Chemistry*, **26**, 2525-2525.
73. Pallenberg, A.J., Dobhal, M.P. and Pandey, R.K. (2004) Efficient synthesis of pyropheophorbide-a and its derivatives. *Organic Process Research & Development*, **8**, 287-290.
74. Zheng, G., Li, H., Zhang, M., Lund-Katz, S., Chance, B. and Glickson, J.D. (2002) Low-density lipoprotein reconstituted by pyropheophorbide cholesteryl oleate as target-specific photosensitizer. *Bioconjugate Chemistry*, **13**, 392-396.
75. Prowse, W. and Maxwell, J. (1991) High molecular weight chlorins in a lacustrine shale. *Organic Geochemistry*, **17**, 877-886.
76. King, L.L. and Repeta, D.J. (1991) Novel pyropheophorbide steryl esters in Black Sea sediments. *Geochimica et Cosmochimica Acta*, **55**, 2067-2074.
77. Chillier, X.F.D., Van Berkel, G.J., Gülaçar, F.O. and Buchs, A. (1994) Characterization of chlorins within a natural chlorin mixture using electrospray/ion trap mass spectrometry. *Organic Mass Spectrometry*, **29**, 672-678.
78. Moulin, M. and Smith, A.G. (2008) Photosynthesis. Energy from the Sun. Springer, pp. 1215-1222.
79. Wilson, M.A., Keely, B.J. (2004) Structure elucidation by LC-MS and multistage mass spectrometry. *Eleventh ISMAS Workshop on Mass Spectrometry,* pp. 95-105.
80. Johnson, D.W. (2001) Analysis of alcohols, as dimethylglycine esters, by electrospray ionization tandem mass spectrometry. *Journal of Mass Spectrometry*, **36**, 277-283.
81. Chen, L., Xiao, Q., Zhang, X. and Yang, J. (2016) Establishment and comparison of three novel methods for the determination of the photodynamic therapy agent 2-[1-hexyloxyethyl]-2-devinyl pyropheophorbide-a (HPPH) in human serum. *Journal of Pharmaceutical and Biomedical Analysis*, **121**, 13-21.
82. Stieger, N., Liebenberg, W. and Wessels, J. (2009) UV spectrophotometric method for the identification and solubility determination of nevirapine. *Die Pharmazie-An International Journal of Pharmaceutical Sciences*, **64**, 690-691.